Astronomy & Astrophysics manuscript no. bensby
August 22, 2011
© ESO 2011

arXiv:1107.5606v2 [astro-ph.GA] 19 Aug 2011

Chemical evolution of the Galactic bulge as traced by microlensed dwarf and subgiant stars⋆,⋆⋆

IV. Two bulge populations

T. Bensby[1,2], D. Adén[1], J. Meléndez[3], A. Gould[4], S. Feltzing[1], M. Asplund[5], J.A. Johnson[4⋆⋆⋆], S. Lucatello[6], J.C. Yee[4], I. Ramírez[7], J.G. Cohen[8], I. Thompson[7], I.A. Bond[9], A. Gal-Yam[10], C. Han[11], T. Sumi[12], D. Suzuki[12], K. Wada[12], N. Miyake[13], K. Furusawa[13], K. Ohmori[13], To. Saito[14], P. Tristram[15], and D. Bennett[16]

[1] Lund Observatory, Department of Astronomy and Theoretical Physics, Box 43, SE-221 00 Lund, Sweden
[2] European Southern Observatory, Alonso de Cordova 3107, Vitacura, Casilla 19001, Santiago 19, Chile
[3] Departamento de Astronomia do IAG/USP, Universidade de São Paulo, Rua do Matão 1226, São Paulo, 05508-900, SP, Brasil
[4] Department of Astronomy, Ohio State University, 140 W. 18th Avenue, Columbus, OH 43210, USA
[5] Max Planck Institute for Astrophysics, Postfach 1317, 85741 Garching, Germany
[6] INAF-Astronomical Observatory of Padova, Vicolo dell'Osservatorio 5, 35122 Padova, Italy
[7] Carnegie Observatories, 813 Santa Barbara Street, Pasadena, CA 91101, USA
[8] Palomar Observatory, Mail Stop 249-17, California Institute of Technology, Pasadena, CA 91125, USA
[9] Institute of Information and Mathematical Sciences, Massey University, Albany Campus, Private Bag 102-904, North Shore Mail Centre, Auckland, New Zealand
[10] Benoziyo Center for Astrophysics, Weizmann Institute of Science, 76100 Rehovot, Israel
[11] Department of Physics, Chungbuk National University, Cheongju 361-763, Republic of Korea
[12] Department of Earth and Space Science, Osaka University, Osaka 560-0043, Japan
[13] Solar-Terrestrial Enivironment Laboratory, Nagoya University, Furo-cho, Chikusa-ku, Nagoya, 464-8601, Japan
[14] Tokyo Metropolitan College of Industrial Technology, Tokyo 116-8523, Japan
[15] Department of Physics, University of Auckland, Private Bag 92019, Auckland 1142, New Zealand
[16] Department of Physics, University of Notre Dame, Notre Dame, IN 46556, USA

Received 11 April 2011 / Accepted 26 July 2011

ABSTRACT

Based on high-resolution ($R \approx 42\,000$ to $48\,000$) and high signal-to-noise ($S/N \approx 50$ to 150) spectra obtained with UVES/VLT, we present detailed elemental abundances (O, Na, Mg, Al, Si, Ca, Ti, Cr, Fe, Ni, Zn, Y, and Ba) and stellar ages for 12 new microlensed dwarf and subgiant stars in the Galactic bulge. Including previous microlensing events, the sample of homogeneously analysed bulge dwarfs has now grown to 26. The analysis is based on equivalent width measurements and standard 1-D LTE MARCS model stellar atmospheres. We also present NLTE Li abundances based on line synthesis of the ^{7}Li line at 670.8 nm. The results from the 26 microlensed dwarf and subgiant stars show that the bulge metallicity distribution (MDF) is double-peaked; one peak at [Fe/H] ≈ -0.6 and one at [Fe/H] $\approx +0.3$, and with a dearth of stars around solar metallicity. This is in contrast to the MDF derived from red giants in Baade's window, which peaks at this exact value. A simple significance test shows that it is extremely unlikely to have such a gap in the microlensed dwarf star MDF if the dwarf stars are drawn from the giant star MDF. To resolve this issue we discuss several possibilities, but we can not settle on a conclusive solution for the observed differences. We further find that the metal-poor bulge dwarf stars are predominantly old with ages greater than 10 Gyr, while the metal-rich bulge dwarf stars show a wide range of ages. The metal-poor bulge sample is very similar to the Galactic thick disk in terms of average metallicity, elemental abundance trends, and stellar ages. Speculatively, the metal-rich bulge population might be the manifestation of the inner thin disk. If so, the two bulge populations could support the recent findings, based on kinematics, that there are no signatures of a classical bulge and that the Milky Way is a pure-disk galaxy. Also, recent claims of a flat IMF in the bulge based on the MDF of giant stars may have to be revised based on the MDF and abundance trends probed by our microlensed dwarf stars.

Key words. Gravitational lensing: micro — Galaxy: bulge — Galaxy: formation — Galaxy: evolution — Stars: abundances

1. Introduction

Almost 60 % of all stellar mass in massive galaxies in the local Universe is contained in bulges and elliptical galaxies (e.g., Gadotti 2009). Being a major component of nearby galaxies and galaxy populations and a primary feature that classifies galaxies,

Send offprint requests to: T. Bensby, e-mail: tbensby@astro.lu.se

⋆ Based on observations made with the European Southern Observatory telescopes (84.B-0837, 85.B-0399, and 86.B-0757). This paper also includes data gathered with the 6.5 m Magellan Telescopes located at the Las Campanas Observatory, Chile, and data obtained at the W.M. Keck Observatory, which is operated as a scientific partnership among the California Institute of Technology, the University of California and the National Aeronautics and Space Administration.

⋆⋆ Table 4 is also available in electronic form at the CDS and full Table 5 is only available in electronic form at the CDS via anonymous ftp to cdsarc.u-strasbg.fr (130.79.128.5) or via http://cdsweb.u-strasbg.fr/cgi-bin/qcat?J/A+A/XXX/AXX.

⋆⋆⋆ J.A. Johnson is a guest professor at Lund University

it is clear that understanding the origin and evolution of bulges is integral to the theory of galaxy formation. The central part of our own Milky Way harbours a central bulge which enables us to study such a stellar system in a detail impossible for any other galaxy (e.g., Kormendy & Kennicutt 2004 for a review of bulges in general). For instance, the next closest bulge stellar system is that of the Andromeda galaxy which is more than a hundred times more distant. In spite of its "proximity" and the many detailed spectroscopic and photometric studies during the last few decades, the origin and evolutionary history of the Galactic bulge is still poorly understood. Its generally very old stellar population, metal-rich nature, and over-abundances of α-elements (e.g., McWilliam & Rich 1994; Zoccali et al. 2006; Fulbright et al. 2007; Meléndez et al. 2008; Bensby et al. 2010c) are consistent with a classical bulge formed during the collapse of the protogalaxy and subsequent mergers, which would have resulted in an intense burst of star formation (e.g., White & Rees 1978; Matteucci & Brocato 1990; Ferreras et al. 2003; Rahimi et al. 2010). Alternatively, the boxy/peanut-like shape of the bulge suggests an origin through dynamical instabilities in an already established inner disk (e.g., Maihara et al. 1978; Combes et al. 1990; Shen et al. 2010). Such secular evolution could possibly explain the recent discovery of chemical similarities between the bulge and the Galactic thick disk as observed in the solar neighbourhood (Meléndez et al. 2008; Alves-Brito et al. 2010; Bensby et al. 2010c; Gonzalez et al. 2011), through the action of radial migration of stars (Sellwood & Binney 2002; Schönrich & Binney 2009; Loebman et al. 2011).

The metallicity distribution function of the bulge, inferred from photometric and spectroscopic studies of red giant stars, peaks around the solar value with a significant fraction of super-solar metallicity stars and a low-metallicity tail extending down to at least [Fe/H]≈ -1 (e.g., Sadler et al. 1996; Zoccali et al. 2003, 2008; Fulbright et al. 2007). Indeed, there are ample indications that the Bulge should harbour substantially more metal-poor stars (e.g., Bensby et al. 2010b). In fact, the very first stars, should any have survived to the present day, may well preferentially be found in the central regions of Milky Way-type galaxies (e.g., Wyse & Gilmore 1992; Brook et al. 2007; Tumlinson 2010). Unfortunately, the high stellar densities in the bulge and its generally high metallicity makes finding such stellar survivors from the earliest cosmic epochs very challenging although several large-scale spectroscopic surveys of the Bulge are currently underway, which may discover some of these extremely old stars (e.g., Howard et al. 2009).

Studies of the detailed chemistry of the bulge have so far mainly used intrinsically bright stars (as in the references above). However, results based on spectra from giant stars are not trivial to interpret as evolutionary processes erase some of the abundance information. Also, their relatively cool atmospheres result in spectra rich in lines from molecules, which are difficult to analyse (e.g., Fulbright et al. 2006). The spectra of dwarf stars, on the other hand, even metal-rich ones, are fairly straightforward to analyse and are the best tracers of Galactic chemical evolution (e.g., Edvardsson et al. 1993). The main difficulty with observing dwarf stars in the bulge is their faintness ($V = 19-20$, Feltzing & Gilmore 2000), impeding spectroscopic observations under normal circumstances. To obtain a spectrum of high quality ($R \gtrsim 40\,000$ and $S/N \gtrsim 75$) of a bulge dwarf star would require, even if using the largest 8-10 meter telescopes available today, an exposure time of more than 50 hours. Microlensing offers the unique opportunity to observe dwarf stars in the bulge. In the event that the bulge dwarf star is lensed by a foreground object, its brightness can increase by a factor of several hundred, making it possible to obtain, in 1 to 2 hours, a spectrum of sufficiently high resolution and S/N, adequate for an accurate detailed elemental abundance analysis.

By observing microlensed dwarf stars in the bulge several recent studies have given a new perspective on the chemical properties of the bulge (Johnson et al. 2007, 2008; Cohen et al. 2008, 2009, 2010; Bensby et al. 2009a,b, 2010b,c; Epstein et al. 2010). Main findings so far include the first age-metallicity relation in the bulge which shows that metal-poor stars are generally old, but metal-rich ones have a wide range of ages (Bensby et al. 2010c). In addition, abundance ratios for 14 elements studied in the bulge dwarfs at sub-solar metallicities are in excellent agreement with the abundance patterns in local thick disk stars (e.g., Meléndez et al. 2008; Bensby et al. 2010c; Alves-Brito et al. 2010). Also, Bensby et al. (2010b) presented the first clear detection of Li in a bulge dwarf star, showing that the bulge follows the Spite plateau (Spite & Spite 1982). The most striking result to date from microlensed dwarf stars is that the metallicity distribution function (MDF) for dwarf stars and giant stars in the Galactic bulge differs. In Bensby et al. (2010c) we found that the bulge MDF appeared bimodal for the dwarf stars, with a paucity at the metallicity where the MDF based on giant stars in Baade's window from Zoccali et al. (2008) peaks. Understanding this discrepancy is vital when studying external galaxies where dwarf stars can not be studied, where we have to rely on the integrated light from all stars, which is dominated by giant stars.

These results illustrate that observations of dwarf stars provide unique information on the evolution of the bulge. For example, the microlensed bulge dwarf stars will have an important impact on the modelling of the bulge, in particular regarding recent suggestions that the initial mass function (IMF) in the bulge needs to be different from that in the solar neighbourhood in order to explain the MDF based on red giant stars (Cescutti & Matteucci 2011). Additionally, combining the dwarf abundances and kinematics with numerical studies, e.g., Rahimi et al. (2010), points to the possibility of disentangling different formation scenarios for the bulge, e.g. secular versus merger origin.

In this paper we report the most recent findings from our ongoing project on the chemical evolution of the Galactic bulge as traced by dwarf and subgiant stars that have been observed whilst being optically magnified during microlensing events. Adding eleven new events, and a re-analysis of MOA-2009-BLG-259S, the sample now consists of in total 26 microlensed dwarf and subgiant stars in the bulge that have been homogeneously analysed.

2. Observations and data reduction

The twelve (11 new and one re-analysis) microlensing events presented in this study were all discovered by the MOA microlensing alert system[1] (e.g., Bond et al. 2001). Most stars were observed on the night when the microlensing events peaked, and as close to peak brightness ($A_{\rm max}$) as possible (the light curves are shown in Fig. 1). Exceptions are MOA-2009-BLG-174S and MOA-2011-BLG-058S which were observed one day ahead of peak brightness as the full Moon would be very close on the night of the predicted $A_{\rm max}$. As can be seen in Fig. 1, the brightnesses for most events were almost constant, or only slowly varying, when the spectroscopic observations were carried out.

[1] https://it019909.massey.ac.nz/moa/alert/index.html

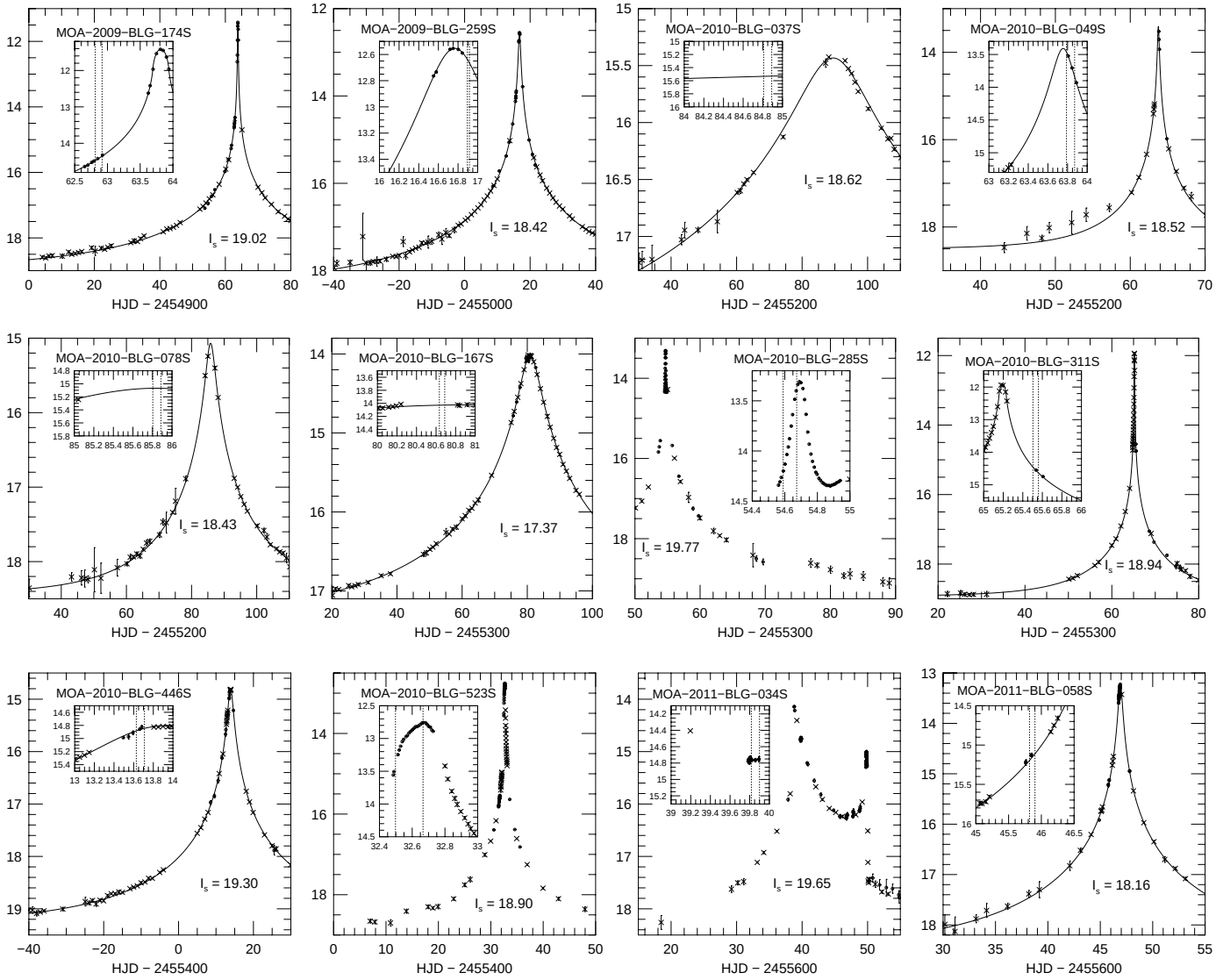

Fig. 1. Light curves for the twelve new microlensing events. Each plot has a zoom window, showing the time intervals when the source stars were observed with high-resolution spectrographs. In each plot the un-lensed magnitude of the source star is also given (I_S).

The event that showed most variation during the observations is MOA-2010-BLG-285S; from $I \approx 14.3$ at the start of the 2 hour exposure to $I \approx 13.3$ at the end, i.e., it more than doubled its brightness during the observations. Furthermore, this microlensing event has a binary lens and the UVES observations were carried out during, or very close to, a caustic crossing. In Bensby et al. (2010b), where we presented the first results for MOA-2010-BLG-285S and reported its Li abundance, we showed that even though the three UVES exposures not only differed in magnification, but also in magnification across the stellar surface, the joint effect is an even magnification across the stellar surface. Hence, the final co-added spectrum should not be affected. As the model light curve for this event requires more analysis, which will be published elsewhere, the light curve in Fig. 1 currently only contains the observed data points and no model fit. Due to a possible planet detection in the lens, the model light curve for MOA-2010-BLG-523S also needs more analysis, and therefore also only have observed data points in Fig. 1. MOA-2011-BLG-034S is an event with a binary lens and the microlensing model needs more work. Hence, we have currently no A_{max}, T_E, or model curve (but only the observed data points in Fig. 1) for MOA-2011-BLG-2011-034S.

Ten of the twelve events were observed in 2010 and 2011 with the UVES spectrograph (Dekker et al. 2000) on the Very Large Telescope as part of our ongoing Target of Opportunity (ToO) program. They were observed with a 1.0 arcsec wide slit and dichroic #2, giving spectra with a resolution of $R \approx 42\,000$ and a spectral coverage between 3760-4980 Å (blue ccd), 5680-7500 Å (lower red ccd), and 7660-9460 Å (upper red ccd). A featureless spectrum of a rapidly rotating B star (either HR 6141 or HR 7830) was obtained each time. This spectrum was used to divide out telluric lines in the bulge star spectrum. The signal-to-noise ratios at 6400 Å are listed in Table 1 and range between 35 and 150. Reductions were carried out with the UVES pipeline (Ballester et al. 2000), version 4.7.8, using the gasgano interface.

The UVES data were complemented with data for two stars observed in 2009. MOA-2009-BLG-259S was observed with the HIRES-R spectrograph (Vogt et al. 1994) on the Keck telescopes

Table 1. Summary of the twelve microlensing events in the Bulge presented in this study[†].

Object	RAJ2000 [hh:mm:ss]	DEJ2000 [dd:mm:ss]	l [deg]	b [deg]	T_E [days]	T_{max} [HJD]	A_{max}	T_{obs} [MJD]	Exp. [s]	S/N	Spec.	R
MOA-2009-BLG-174S	18:02:07.70	−31:25:26.40	−0.34	−4.34	65	4963.8147	1100	4962.314	9000	95	MIKE	42 000
MOA-2009-BLG-259S	17:57:57.50	−29:11:39.00	1.15	−2.45	62	5016.7674	204	5016.395	1800	110	HIRES	48 000
MOA-2010-BLG-037S	18:05:17.93	−27:56:13.21	3.04	−3.23	92	5289.4614	19	5284.308	7200	35	UVES	42 000
MOA-2010-BLG-049S	18:05:07.02	−26:46:12.79	4.04	−2.63	12	5263.7554	110	5263.289	7200	90	UVES	42 000
MOA-2010-BLG-078S	17:52:01.65	−30:24:25.63	−0.64	−1.95	30	5285.8370	22	5285.303	7200	40	UVES	42 000
MOA-2010-BLG-167S	18:11:27.37	−29:41:02.54	2.16	−5.26	65	5380.8834	22	5380.129	4740	100	UVES	42 000
MOA-2010-BLG-285S	17:56:48.16	−30:00:39.47	0.32	−2.64	42	4354.7421	390	5354.087	7200	150	UVES	42 000
MOA-2010-BLG-311S	18:08:49.98	−25:57:04.27	5.17	−2.96	19	5365.1937	540	5365.001	4800	55	UVES	42 000
MOA-2010-BLG-446S	18:07:04.25	−28:03:57.77	3.12	−3.64	20	5413.8937	61	5413.125	7200	70	UVES	42 000
MOA-2010-BLG-523S	17:57:08.87	−29:44:58.40	0.58	−2.58	20	5432.6283	290	5431.997	7200	150	UVES	42 000
MOA-2011-BLG-034S	18:10:12.23	−27:32:02.39	3.92	−3.99	–	5638.62	–	5639.317	7200	45	UVES	42 000
MOA-2011-BLG-058S	18:09:00.36	−29:14:12.66	2.30	−4.57	17	5646.92	90	5645.320	7200	45	UVES	42 000

Notes. [†] Given for each microlensing event is: RA and DE coordinates (J2000) read from the fits headers of the spectra (the direction where the telescope pointed during observation); galactic coordinates (l and b); duration of the event in days (T_E); time when maximum magnification occured (T_{max}); maximum magnification (A_{max}); time when the event was observed with high-resolution spectrograph (T_{obs}); the exposure time (Exp.), the measured signal-to-noise ration per pixel at ∼6400 Å (S/N); the spectrograph that was used (Spec); the spectral resolution (R).

Table 2. Stellar parameters and radial velocities for the 12 new microlensed dwarf stars.[†]

Object	$T_{\rm eff}$ [K]	$\log g$ [cgs]	$\xi_{\rm t}$ [km s^{-1}]	[Fe/H]	$N_{\rm Fe\,I,\,Fe\,II}$	$v_{\rm r}$ [km/s]
MOA-2010-BLG-285S	6064 ± 129	4.20 ± 0.23	1.85 ± 0.38	−1.23 ± 0.09	53, 12	+46.0
MOA-2010-BLG-078S	5231 ± 135	3.60 ± 0.31	1.30 ± 0.29	−0.99 ± 0.15	54, 3	+52.3
MOA-2010-BLG-167S	5444 ± 58	4.00 ± 0.14	1.17 ± 0.11	−0.59 ± 0.05	118, 17	−79.4
MOA-2010-BLG-049S	5738 ± 58	4.20 ± 0.12	0.95 ± 0.11	−0.38 ± 0.06	96, 14	−116.7
MOA-2010-BLG-446S	6327 ± 123	4.50 ± 0.19	1.57 ± 0.17	−0.37 ± 0.08	69, 8	+56.5
MOA-2010-BLG-523S	5250 ± 98	4.00 ± 0.23	2.10 ± 0.24	+0.10 ± 0.07	54, 11	+97.3
MOA-2009-BLG-174S	5620 ± 65	4.40 ± 0.12	1.23 ± 0.11	+0.13 ± 0.05	121, 17	−21.4
MOA-2011-BLG-034S	5467 ± 67	4.10 ± 0.15	0.87 ± 0.14	+0.13 ± 0.06	84, 11	+127.0
MOA-2009-BLG-259S	4953 ± 93	3.40 ± 0.24	1.02 ± 0.11	+0.37 ± 0.05	72, 11	+81.5
MOA-2011-BLG-058S	5260 ± 75	4.00 ± 0.16	0.67 ± 0.14	+0.39 ± 0.05	63, 10	−139.7
MOA-2010-BLG-311S	5464 ± 108	3.80 ± 0.26	1.29 ± 0.19	+0.49 ± 0.11	58, 11	+44.4
MOA-2010-BLG-037S	5745 ± 95	4.00 ± 0.26	1.51 ± 0.20	+0.56 ± 0.10	56, 13	−8.4

Notes. [†] Given for each star is: effective temperature ($T_{\rm eff}$); surface gravity ($\log g$); microturbulence parameter ($\xi_{\rm t}$); [Fe/H]; number of Fe I and Fe II lines used in the analysis; radial velicity ($v_{\rm r}$).

on Hawaii. The slit was 0.86 arcsec wide, giving a spectral resolution of $R \approx 48\,000$, a wavelength coverage from 3900 to 8350 Å, with small gaps between the orders beyond 6650 Å. The signal-to-noise ratio is $S/N \approx 110$ per pixel around 6400 Å. Details of the reduction procedure can be found in Cohen et al. (2008). Actually, an analysis of MOA-2009-BLG-259S was first presented in Bensby et al. (2010c). However, that analysis was based on a spectrum that was obtained with UVES and when only the UVES blue arm was available due to maintenance work on the red arm. That spectrum had a very limited blue wavelength coverage and as bulge stars are heavily reddened, it also had poor S/N. As a result only a few Fe I and Fe II could be measured and the stellar parameters were poorly constrained with large uncertainties. Hence, in Bensby et al. (2010c), MOA-2009-BLG-259S was excluded when discussing the metallicity distribution and abundance trends of the microlensed bulge dwarf stars. The first metallicity result, based on this HIRES spectrum, was presented in Cohen et al. (2010). For consistency, it has here been re-analysed with the same methods as for all the other events.

MOA-2009-BLG-174S was observed with the MIKE spectrograph (Bernstein et al. 2003) on the Magellan Clay telescope at the Las Campanas observatory in Chile. A 0.7 arcsec wide slit was used giving a spectrum with $R \approx 42\,000$ and continuous coverage between 3500 to 9200 Å. The signal-to-noise per pixel at 6400 Å is around 95. Reductions were made with the Carnegie python pipeline[2].

In total we are now in possession of high quality spectra for 26 microlensed dwarf and subgiant stars in the bulge. Table 1 lists the details for the twelve new events, while the data for the other 14 events can be found in Bensby et al. (2010c).

3. Analysis

3.1. Stellar parameters and elemental abundances

Stellar parameters and elemental abundances have been determined through exactly the same methods as in our previous studies of microlensed bulge dwarfs (Bensby et al. 2009b, 2010c). Briefly, we use standard 1-D plane-parallel model stel-

[2] Available at `http://obs.carnegiescience.edu/Code/mike`

Table 3. Stellar ages and a comparison of colours and effective temperatures as determined from spectroscopy and microlensing techniques for all 26 microlensed dwarf stars. The lower part of the table includes the stars from Bensby et al. (2010c).†

Object	$T_{\rm eff}$ [K]	$\mathcal{M}$ $M_\odot$	$\log L$ $L_\odot$	Age [Gyr]	-1σ [Gyr]	$+1\sigma$ [Gyr]	$(V–I)_0$ [mag]	M_V [mag]	-1σ [mag]	$+1\sigma$ [mag]	M_I [mag]	M_I^μ [mag]	$(V–I)_0^\mu$ [mag]	$T_{\rm eff}^\mu$ [K]	Comments
MOA-2010-BLG-285S	6064	0.81	0.04	11.6	7.4	13.3	0.63	4.80	3.78	5.06	4.18	4.84	0.58	6283	
MOA-2010-BLG-078S	5231	0.84	0.75	12.7	5.0	15.5	0.86	3.04	2.23	3.45	2.18	1.86	0.85	5259	very high DR
MOA-2010-BLG-167S	5444	0.87	0.34	14.0	8.6	15.1	0.79	4.03	3.61	4.11	3.24	2.78	0.72	5678	
MOA-2010-BLG-049S	5738	0.88	0.16	11.7	9.7	13.3	0.70	4.46	4.10	4.84	3.76	2.74	0.69	5785	some DR
MOA-2010-BLG-446S	6327	1.06	0.23	3.2	1.4	4.7	0.56	4.11	3.81	4.45	3.55	–	–	–	a bit of DR, corrupt CMD
MOA-2010-BLG-523S	5250	0.99	0.26	13.1	5.5	13.2	0.86	4.29	3.60	4.67	3.43	–	0.77	5510	a bit of DR
MOA-2009-BLG-174S	5620	0.98	–0.05	8.7	3.8	9.7	0.73	4.99	4.62	5.12	4.26	3.57	0.71	5703	
MOA-2011-BLG-034S	5467	0.96	0.17	11.6	8.0	13.2	0.77	4.46	3.85	4.86	3.69		0.67	5720	
MOA-2009-BLG-259S	4953	1.21	0.79	3.0	1.8	7.7	1.00	3.03	2.09	3.89	2.03	2.95	0.82	5366	
MOA-2011-BLG-058S	5260	0.97	0.34	12.7	6.4	13.1	0.85	4.08	3.77	4.66	3.23	3.36	0.82	5366	
MOA-2010-BLG-311S	5464	1.09	0.39	4.9	3.1	9.1	0.78	3.92	2.81	4.50	3.14	3.21	0.75	5568	high DR
MOA-2010-BLG-037S	5745	1.25	0.49	4.4	2.9	5.5	0.69	3.63	2.98	4.30	2.94	3.61	0.80	5421	
OGLE-2009-BLG-076S	5877	0.84	–0.04	11.6	7.0	13.1	0.67	5.00	4.26	5.17	4.33	4.24	0.70	5752	
MOA-2009-BLG-493S	5457	0.74	–0.41	13.1	4.3	13.1	0.79	5.83	5.59	6.11	5.04	4.81	0.70	5752	some DR
MOA-2009-BLG-133S	5597	0.81	–0.24	12.1	5.0	15.9	0.74	5.54	4.70	5.77	4.80	4.24	0.71	5715	double clump sightline
MOA-2009-BLG-475S	5843	0.85	–0.08	8.7	4.5	12.3	0.68	5.10	4.12	5.33	4.42	4.30	0.62	6070	some DR
MACHO-1999-BLG-022S	5650	0.88	0.36	13.1	7.0	13.4	0.73	3.97	3.49	4.70	3.24	–	–	–	
OGLE-2008-BLG-209S	5243	0.93	0.38	8.6	5.3	12.7	0.86	3.96	3.34	4.11	3.10	2.57	0.76	5542	
MOA-2009-BLG-489S	5643	0.93	–0.09	11.6	6.1	12.8	0.73	4.97	4.33	5.22	4.24	3.44	0.88	5200	high DR
MOA-2009-BLG-456S	5700	1.00	0.05	8.7	4.9	9.9	0.71	4.59	4.00	4.90	4.88	2.81	0.69	5773	
OGLE-2007-BLG-514S	5635	1.06	0.16	6.4	4.2	9.6	0.73	4.49	3.53	4.87	3.76	4.41	0.73	5634	high DR, binary peak
MOA-2008-BLG-311S	5944	1.17	0.18	2.9	1.1	3.5	0.64	4.37	4.06	4.51	3.73	3.98	0.69	5767	a bit of DR
MOA-2006-BLG-099S	5741	1.10	0.04	3.3	1.5	5.0	0.70	4.66	4.35	4.87	3.96	3.86	0.77	5508	very high DR
MOA-2008-BLG-310S	5704	1.09	0.07	4.9	3.0	6.3	0.71	4.69	4.04	4.76	3.98	3.51	0.72	5664	Janczak et al. (2010)
OGLE-2007-BLG-349S	5229	0.95	0.15	13.1	9.6	13.9	0.87	4.58	4.34	5.30	3.71	4.21	0.81	5393	a bit of DR
OGLE-2006-BLG-265S	5486	1.04	0.10	8.7	5.4	9.5	0.78	4.65	4.23	5.00	3.87	3.64	0.71	5696	

Notes. † Column 2 gives the spectroscopic temperature; col. 3 the stellar mass (inferred from ischrones); col. 4 the luminosity (inferred from isochrones), col. 5 the stellar age (inferred from isochrones); cols. 6 and 7 the 1-sigma lower and upper age limits; col. 8 the "spectroscopic" colours, based on the colour–[Fe/H]–$T_{\rm eff}$ calibrations by Casagrande et al. (2010); col. 9 the absolute V magnitude based on the spectroscopic stellar parameters; cols. 10 and 11 the 1-sigma lower and upper limits on M_V; col. 12 the absolute I magnitude based on spectroscopic stellar parameters; col. 13 the absolute I magnitude based on microlensing techniques; col. 14 the $(V-I)_0$ colour based on microlensing techniques; col. 15 the inferred effective temperatures using the colour–[Fe/H]–$T_{\rm eff}$ calibrations by Casagrande et al. (2010); col. 16 Comments: DR stands for differential reddening.

Table 5. Measured equivalent widths and calculated elemental abundances for the 12 new microlensed dwarfs.†

Element	λ	χ_1	star 1		⋯	star 10	
	[Å]	[eV]	W_λ	$\epsilon(X)$	⋯	W_λ	$\epsilon(X)$
⋮	⋮	⋮	⋮	⋮	⋯	⋮	⋮

† For each line we give the $\log gf$ value, lower excitation energy (χ_1), equivalent width (W_λ), absolute abundance ($\log\epsilon(X)$). The table is only available in electronic form at the CDS via anonymous ftp to `cdsarc.u-strasbg.fr (130.79.128.5)` or via `http://cdsweb.u-strasbg.fr/cgi-bin/qcat?J/A+A/XXX/AXX`.

Table 6. LTE Li abundances and NLTE corrections from Lind et al. (2009).

Object	$\log\epsilon(\rm Li)_{\rm LTE}$	$\Delta_{\rm NLTE}$	$T_{\rm eff}$ [K]	[Fe/H]
OGLE-2006-BLG-265S†	0.96	+0.08	5486	+0.47
OGLE-2007-BLG-349S†	0.89	+0.11	5229	+0.42
MOA-2008-BLG-311S†	2.23	+0.01	5944	+0.36
MOA-2010-BLG-049S	1.43	+0.07	5738	−0.38
MOA-2010-BLG-285S	2.21	−0.05	6064	−1.23
MOA-2010-BLG-523S	1.64	+0.10	5250	+0.09

† Full set of stellar parameters and elemental abundances for OGLE-2006-BLG-265S, OGLE-2007-BLG-349S, and MOA-2008-BLG-311S are given in Bensby et al. (2010c).

lar atmospheres calculated with the Uppsala MARCS code (Gustafsson et al. 1975; Edvardsson et al. 1993; Asplund et al. 1997). (For consistency with our previous analyses, we continue to use the old MARCS models. As shown in Gustafsson et al. 2008, the differences between the new and old MARCS models are very small for our types of stars, i.e. F and G dwarf stars.) Elemental abundances are calculated with the Uppsala EQWIDTH program using equivalent widths that were measured by hand using the IRAF task SPLOT. Effective temperatures were determined from excitation balance of abundances from Fe I lines, surface gravities from ionisation balance between abundances from Fe I and Fe II lines, and the microturbulence parameters by requiring that the abundances from Fe I lines are independent of line strength.

An error analysis, as outlined in Epstein et al. (2010), has been performed for the microlensed dwarf stars. This method takes into account the uncertainties in the four observables that were used to find the stellar parameters, i.e. the uncertainty of the slope in the graph of Fe I abundances versus lower excitation potential; the uncertainty of the slope in the graph of Fe I abundances versus line strength; the uncertainty in the difference between Fe I and Fe II abundances; and the uncertainty in the difference between input and output metallicities. The method also accounts for abundance spreads (line-to-line scatter) as well as

Table 4. Elemental abundance ratios, errors in the abundance ratios, and number of lines used, for the 12 new microlensed dwarf stars[†].

	[Fe/H]	[O/Fe][†]	[Na/Fe]	[Mg/Fe]	[Al/Fe]	[Si/Fe]	[Ca/Fe]	[Ti/Fe]	[Cr/Fe]	[Ni/Fe]	[Zn/Fe]	[Y/Fe]	[Ba/Fe]
MOA-2010-BLG-285S	−1.23	0.55	−0.06	0.42	0.30	0.30	0.35	0.38	−0.01	−0.08	0.28	0.39	0.22
MOA-2010-BLG-078S	−0.99	0.65	−0.02	0.47	0.25	0.35	0.26	0.34	−−	0.00	−−	−−	0.32
MOA-2010-BLG-167S	−0.59	0.56	0.07	0.43	0.33	0.22	0.23	0.34	0.07	0.03	0.14	0.07	−0.18
MOA-2010-BLG-049S	−0.38	0.36	−0.05	0.28	0.28	0.14	0.25	0.31	0.02	0.01	0.23	0.1	0.13
MOA-2010-BLG-446S	−0.37	0.21	0.10	0.32	0.23	0.18	0.25	0.34	−−	0.05	−−	−−	−0.06
MOA-2010-BLG-523S	0.10	0.25	0.19	0.14	0.33	−0.01	0.17	0.22	0.16	0.00	−0.24	−−	−0.18
MOA-2009-BLG-174S	0.13	−0.03	−0.03	0.09	−0.04	0.03	0.02	0.08	0.04	−0.03	−0.05	−0.03	−0.04
MOA-2011-BLG-034S	0.13	−0.11	0.02	0.03	0.07	0.07	−0.01	0.05	−0.02	0.03	0.03	−−	−0.14
MOA-2009-BLG-259S	0.37	0.03	0.42	0.36	0.35	0.10	0.17	0.14	0.11	0.18	0.41	0.38	−0.07
MOA-2011-BLG-058S	0.39	−0.12	0.20	0.11	0.05	0.08	0.00	0.00	0.10	0.13	0.28	–	−0.12
MOA-2010-BLG-311S	0.49	−0.24	0.26	0.24	0.18	0.08	0.13	0.07	0.03	0.14	0.14	−−	−0.13
MOA-2010-BLG-037S	0.56	−0.40	0.31	0.16	0.10	0.08	−0.04	0.14	0.06	0.13	−0.23	−−	−0.10
	$\sigma_{[Fe/H]}$	$\sigma_{[O/Fe]}$	$\sigma_{[Na/Fe]}$	$\sigma_{[Mg/Fe]}$	$\sigma_{[Al/Fe]}$	$\sigma_{[Si/Fe]}$	$\sigma_{[Ca/Fe]}$	$\sigma_{[Ti/Fe]}$	$\sigma_{[Cr/Fe]}$	$\sigma_{[Ni/Fe]}$	$\sigma_{[Zn/Fe]}$	$\sigma_{[Y/Fe]}$	$\sigma_{[Ba/Fe]}$
MOA-2010-BLG-285S	0.095	0.26	0.05	0.07	0.07	0.07	0.06	0.12	0.19	0.11	0.10	0.24	0.21
MOA-2010-BLG-078S	0.15	0.49	0.10	0.13	0.12	0.17	0.19	0.05	−−	0.15	−−	−−	0.14
MOA-2010-BLG-167S	0.05	0.19	0.09	0.08	0.04	0.06	0.09	0.07	0.07	0.06	0.14	0.20	0.09
MOA-2010-BLG-049S	0.06	0.18	0.15	0.06	0.03	0.05	0.10	0.09	0.09	0.06	0.10	0.21	0.08
MOA-2010-BLG-446S	0.08	0.18	0.05	0.06	0.07	0.05	0.07	0.03	−−	0.09	−−	−−	0.24
MOA-2010-BLG-523S	0.07	0.22	0.13	0.12	0.10	0.08	0.15	0.11	0.08	0.07	0.13	−−	0.11
MOA-2009-BLG-174S	0.05	0.15	0.08	0.07	0.05	0.04	0.09	0.07	0.05	0.05	0.12	0.26	0.11
MOA-2011-BLG-034S	0.06	0.19	0.03	0.09	0.06	0.06	0.10	0.07	0.04	0.06	0.14	−−	0.10
MOA-2009-BLG-259S	0.05	0.24	0.22	0.19	0.10	0.08	0.20	0.09	0.07	0.06	0.14	0.57	0.20
MOA-2011-BLG-058S	0.04	0.18	0.09	0.09	0.10	0.06	0.10	0.10	0.08	0.05	0.09	–	0.05
MOA-2010-BLG-311S	0.11	0.27	0.12	0.19	0.14	0.09	0.16	0.09	0.08	0.09	0.17	−−	0.28
MOA-2010-BLG-037S	0.10	0.29	0.16	0.18	0.11	0.07	0.12	0.10	0.12	0.09	0.24	−−	0.28
	$N_{Fe\,I}$	N_O	N_{Na}	N_{Mg}	N_{Al}	N_{Si}	N_{Ca}	N_{Ti}	N_{Cr}	N_{Ni}	N_{Zn}	N_Y	N_{Ba}
MOA-2010-BLG-285S	53	3	1	6	3	13	10	15	3	11	2	3	4
MOA-2010-BLG-078S	54	2	1	4	4	16	10	2	−−	9	−−	−−	2
MOA-2010-BLG-167S	118	3	2	6	6	23	15	25	9	33	3	3	4
MOA-2010-BLG-049S	96	3	2	7	6	25	13	13	2	34	3	2	3
MOA-2010-BLG-446S	69	3	2	5	5	19	10	3	−−	15	−−	−−	3
MOA-2010-BLG-523S	54	3	2	4	6	20	11	2	5	25	1	−−	3
MOA-2009-BLG-174S	122	3	4	4	7	27	18	16	12	34	1	3	3
MOA-2011-BLG-034S	84	3	2	5	6	23	11	6	2	30	1	−−	3
MOA-2009-BLG-259S	64	3	3	3	3	17	11	13	13	29	1	2	2
MOA-2011-BLG-058S	63	2	2	5	6	24	12	6	5	30	1	–	3
MOA-2010-BLG-311S	58	3	2	5	6	27	10	6	5	26	1	−−	3
MOA-2010-BLG-037S	56	3	2	5	6	25	11	6	3	25	1	−−	3

[†] Note that the abundance ratios for oxygen have been corrected for NLTE effects according to the empirical formula given in Bensby et al. (2004b).

how the average abundances for each element reacts to changes in the stellar parameters. Compared to Epstein et al. (2010), who used Ca I lines to constrain the microturbulence parameter, we use the same Fe I lines that were used for the effective temperature. Although the variables are not fully independent, they are only weakly correlated. Thus the total error bar is dominated by the uncertainties in the slopes.

Stellar parameters and error estimates are given in Table 2, elemental abundance ratios in Table 4, and measured equivalent widths and abundances for individual lines in Table 5.

We have also determined NLTE Li abundances in 6 of the 26 microlensed dwarf stars through line profile fitting of the ^{7}Li I resonance doublet line at 670.8 nm. The 1-D NLTE corrections are taken from Lind et al. (2009). The Li line was not detected in the remaining 20 stars, and the spectra are not of sufficient quality to estimate interesting upper limits. The method we use to determine Li abundances is fully described in Bensby et al. (2010b) where we presented the Li abundance in MOA-2010-BLG-285S. The Li abundances are listed in Table 6.

3.2. Stellar ages and absolute magnitudes

The determination of stellar ages has been greatly improved in relation to our previous work, by the use of probability distribution functions. Furthermore, the Yonsei-Yale isochrones (Demarque et al. 2004) have been calibrated to reproduce the solar age and solar mass for the input solar stellar parameters ($T_{\rm eff}/\log g/[Fe/H] = 5777\,K/4.44/0.00$). This is described in detail in a forthcoming paper (Melendez et al., in prep.). In short, for a given set of "observed" stellar parameters ($T_{\rm eff}$, log g, [Fe/H]) and theoretical isochrone points (effective temperature T, logarithm of surface gravity G, and metallicity M), the age is determined from an isochrone age probability distribution (APD):

$$dP(\mathrm{age}) = \frac{1}{\Delta(\mathrm{age})} \sum_{\Delta(\mathrm{age})} p\,(T_{\rm eff}, \log g, [\mathrm{Fe/H}], T, G, M)\,, \qquad (1)$$

where Δ(age) is an adopted step in age from the grid of isochrones and:

$$p \propto \exp[-(T_{\rm eff} - T)^2/2(\Delta T_{\rm eff})^2] \times$$

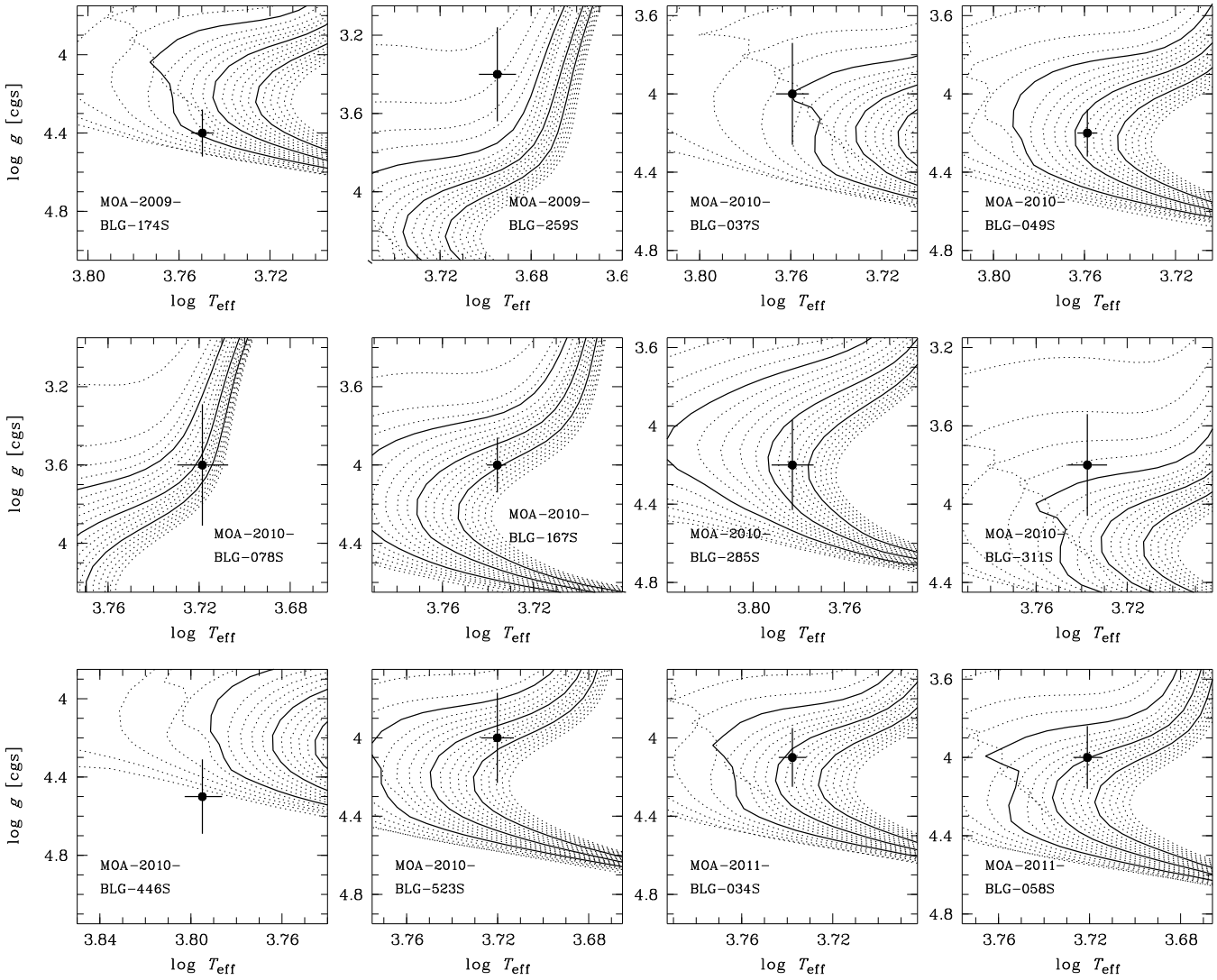

Fig. 2. The 12 new microlensed stars plotted on the α-enhanced isochrones from Demarque et al. (2004). Each set of isochrones have been calculated with the same metallicity and α-enhancement as derived for the stars. In each plot the solid lines represent isochrones with ages of 5, 10, and 15 Gyr (from left to right). Dotted lines are isochrones in steps of 1 Gyr, ranging from 0.1 Gyr to 20 Gyr. Error bars represent the uncertainties in $T_{\rm eff}$ and $\log g$ as given in Table 2. Note that ages reported in Table 3 need not coincide exactly with the ages that may be read off directly from the figures. The age determinations are based on probability distribution functions and is described in Sect. 3.

$$\exp[-(\log g - G)^2/2(\Delta \log g)^2] \times \exp[-([{\rm Fe/H}] - M)^2/2(\Delta[{\rm Fe/H}])^2] \, . \quad (2)$$

The errors in the derived stellar parameters ($\Delta T_{\rm eff}$, etc.) are listed in Table 2. The sum in Eq. (1) is made over a range of isochrone ages and in principle all values of T, G, M. In practice, the contribution to the sum from isochrone points farther away than $T_{\rm eff} \pm 3\Delta T_{\rm eff}$, etc., is negligible. Therefore, the sum is limited to isochrone points within a radius of three times the errors around the observed stellar parameters. The probability distributions are normalised so that $\sum dP = 1$. The most probable age is obtained from the peak of the distribution while $1\,\sigma$ limits are derived from the shape of the probability distribution. Similar formalisms allow us to infer the stellar mass, absolute magnitudes, and luminosities.

For three very old stars (> 12 Gyr), both the peak and the upper error bar of the APD are not well defined. In those cases we adopted as the age the average of the APD peak and the median of the solutions, and the upper error bar was adopted as the scatter of the solutions. The probability distributions for mass, absolute magnitudes, and luminosities are all well behaved.

Using the new improved age determination method we have re-determined the ages for all 26 stars. The ages, absolute magnitudes, and luminosities are reported in Table 3, and Fig. 2 shows the twelve new microlensed dwarf stars together with the relevant Y2 isochrones. As can be seen, a majority of the stars are either main sequence turn-off stars or subgiant stars, while two or three are on the verge of ascending the giant branch. The latter ones have just left the subgiant branch, and should be un-affected by the internal mixing processes that occur further up on the giant branch (see, e.g., Pinsonneault 1997, for a review on mixing in stars).

The masses and luminosities presented in Table 3 will yield a "physical" $\log g$, computed from the fundamental relationship

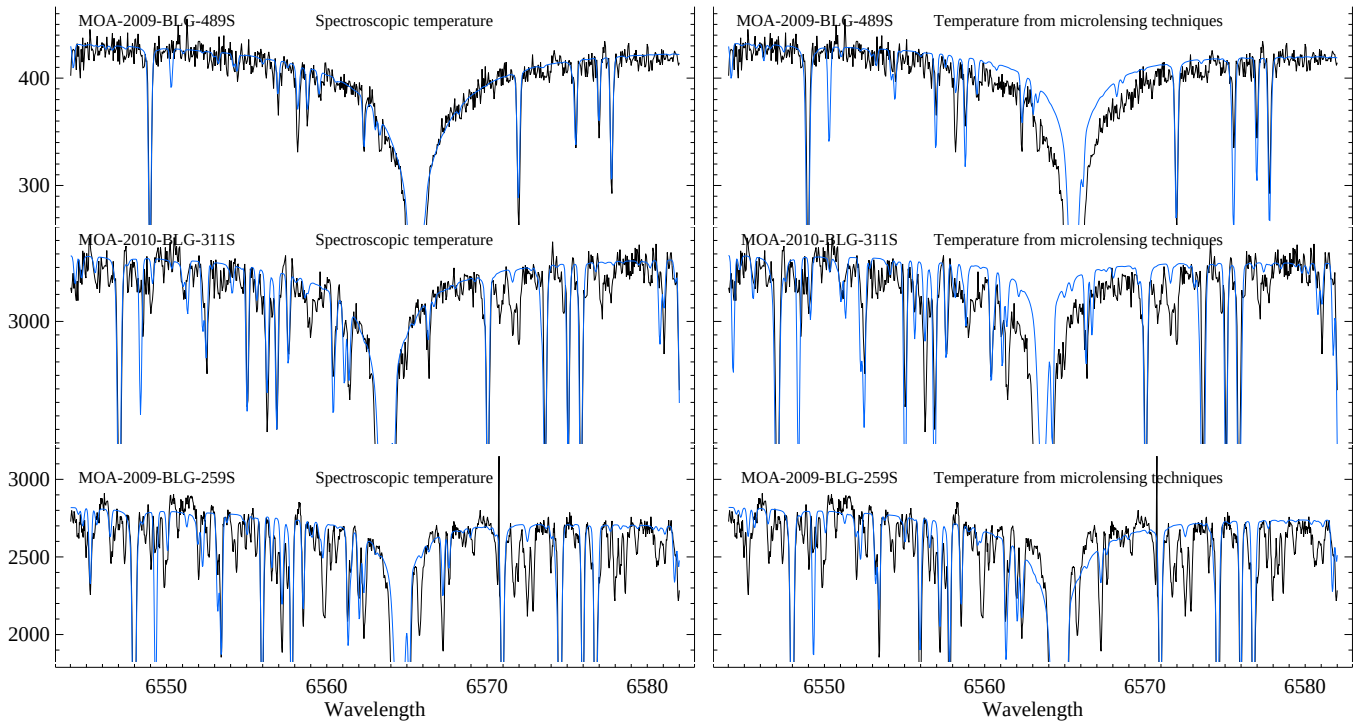

Fig. 3. Synthesis of the Hα line at 6563 Å for the three stars that show large deviations between the spectroscopic effective temperatures and the effective temperatures based on microlensing techniques. Observed spectra are shown with black lines, and the synthetic spectra with blue lines. Left-hand side shows the synthetic profiles based on spectroscopic temperatures and the right-hand side the profiles based on temperatures from microlensing techniques. The microlensing temperature for MOA-2010-BLG-311S is the one based on the original $(V-I)_0$ colour (i.e. $T_{\rm eff}$ = 4750 K). Note that no attempts to match individual lines has been made. The composition of the model atmospheres are simply scaled with [Fe/H] relative to the standard solar composition by Grevesse et al. (2007).

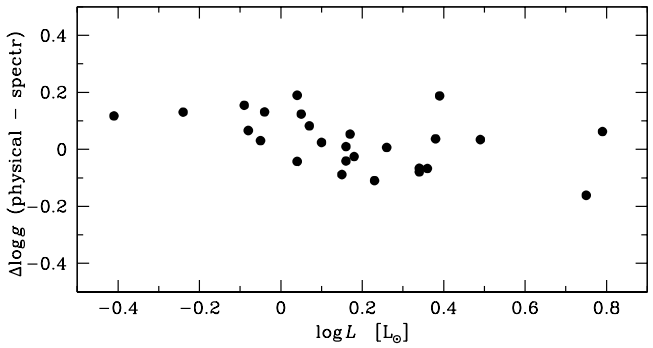

Fig. 4. Comparison between out spectroscopic surface gravities and the "physical" $\log g$ that can be computed from the luminosities and stellar masses inferred from isochrones. On average the physical $\log g$:s are 0.03 dex higher (with a dispersion of 0.09 dex).

that relates luminosity, stellar mass, and effective temperature (see, e.g., Eq. (4) in Bensby et al. 2003). Because a star with the best-fit age may not lie exactly at the spectroscopically measured $T_{\rm eff}$ and $\log g$, the the physical and spectroscopic $\log g$:s agree within 0.03 ± 0.09 dex, rather than exactly, see Fig. 4.

Probabilistic age determinations like ours are known to suffer from systematic biases mainly related to the sampling of isochrone data points (e.g., Nordström et al. 2004, their Sect. 4.5.4). Bayesian methods have been developed to tackle these problems (e.g., Pont & Eyer 2004; Jørgensen & Lindegren 2005; Casagrande et al. 2011) but we do not follow this approach and therefore our ages could be in principle further improved. Nevertheless, our current age determination is consistent with our previous work on thin/thick disk stars so, in a relative sense, our discussions regarding the ages of our sample stars are still reliable.

3.3. Effective temperatures from microlensing techniques

As in Bensby et al. (2010c) we confront the effective temperatures derived from spectroscopic principles with those deduced from microlensing techniques (Yoo et al. 2004). The microlensing method assumes that the reddening towards the microlensed source is the same as the reddening towards the red clump, and that the red clump in the Bulge has $(V-I)_0$ = 1.08 (Bensby et al. 2010c) and M_I = −0.15 (David Nataf, private communication). The de-reddened magnitude and colour are then derived from the offsets between the microlensing source and the red clump, in the instrumental colour-magnitude diagram (CMD). As the lenses for the MOA-2010-BLG-285S and -523S events likely are binaries, and need more work, no absolute magnitudes could be estimated for these stars. Also, the $(V-I)_0$ colour for MOA-2010-BLG-446S could not be determined because there are too few clump stars close to this star in the

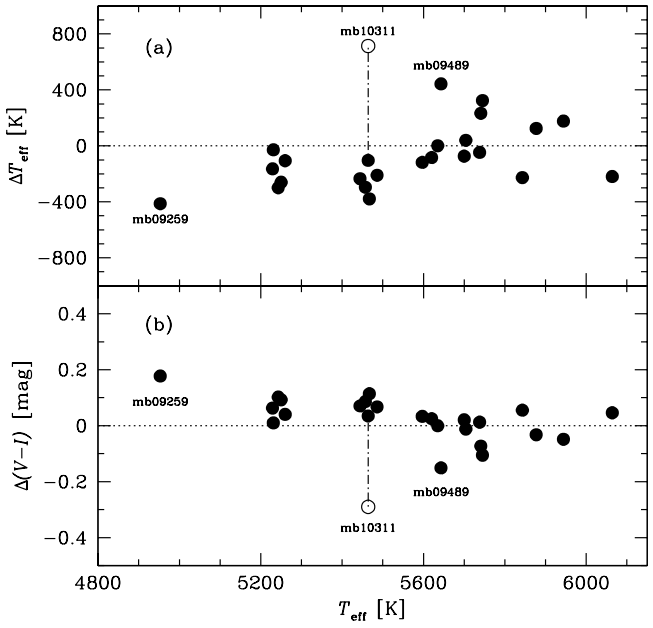

Fig. 5. (a) Difference between the spectroscopic temperatures and the temperatures from microlensing techniques versus effective temperature, and (b) the difference between $(V-I)_0$ colours determined from microlensing techniques and those that can be determined from the spectroscopic temperatures using the *IRFM* calibration by Casagrande et al. (2010). The average differences are $\langle \Delta T_{\rm eff} \rangle = -80$ K with a dispersion of 217 K, and $\langle \Delta(V-I)_0 \rangle = 0.026$ with a dispersion of 0.073 mag. The three stars that show largest deviations between microlensing and spectroscopic parameters are marked. For MOA-2010-BLG-311S (mb10311) the original values are shown with open circles, and the corrected value with filled circles (connected with the original values by a dash-dotted line).

colour-magnitude diagram. From the colour-[Fe/H]-$T_{\rm eff}$ calibrations by Casagrande et al. (2010) we can determine which temperatures the $(V-I)_0$ colours correspond to. The absolute dereddened magnitudes and colours and the effective temperatures are given in Table 3.

Even though the effective temperatures from microlensing techniques and spectroscopic principles are in reasonable agreement, there are three events for which the differences are disturbingly large; more than 400 K for MOA-2009-BLG-259S and MOA-2009-BLG-489S, and more than 700 K for MOA-2010-BLG-311S (Fig. 5a). Note that stellar parameters for MOA-2009-BLG-489S were published in Bensby et al. (2010c). To check the temperatures for these stars, and get a third opinion, we calculate synthetic spectra for the Hα line wing profiles with the latest version (v2.1 oct 2010) of the Spectroscopy Made Easy (SME) tool (Valenti & Piskunov 1996) using the latest 1-D LTE plane-parallel MARCS model stellar atmospheres (Gustafsson et al. 2008), and line data from VALD (Piskunov et al. 1995; Kupka et al. 1999). In Fig. 3 we show the observed line profiles and synthetic line profiles for the Balmer Hα line for these three stars, using both the spectroscopic temperatures (left-hand side plots) and the temperatures from microlensing techniques (right-hand side plots). We see that the synthetic spectra based on spectroscopic temperatures reproduce the wings of the Hα line almost perfectly, while the spectra based on temperatures from microlensing techniques clearly do not match the observed wing profiles.

We could not find anything that was obviously wrong with the photometry of MOA-2009-BLG259S and MOA-2009-BLG-489S, although differential reddening is noticeable in the field of MOA-2009-BLG-489S (Nataf, private communication, see also Table 3). However, for MOA-2010-BLG-311S there was only one highly-magnified V point, so the $(V-I)_0$ colour could not be robustly estimated by the standard techniques used by Yoo et al. (2004). In an alternative attempt to determine the $(V-I)_0$ colour for MOA-2010-BLG-311S we first determined the instrumental $(I-H)$ colour, making use of the H-band data that are simultaneously taken with I band on the SMARTS ANDICAM camera at the 1.3 m CTIO telescope. We then converted from instrumental $(I-H)$ to $(V-I)$ by constructing a VIH colour-colour diagram for field stars, which is analogous to the technique for optical colour transformations (Gould et al. 2010). Now we find a colour of $(V-I)_0 = 0.75$ for MOA-2010-BLG-311S, which is in good agreement with the "spectroscopic" value of 0.78. Note, however, that this method cannot be blindly applied to VIH transformations because (at the depth of the SMARTS H-band images) the colour-colour diagram is constructed from giants and subgiants, while the transformation applies to dwarfs. Additionally, there is a giant-dwarf bifurcation of the VIH colour-colour relations for $(V-K)_0 > 3$ (Bessell & Brett 1988), which corresponds to $(V-I)_0 > 1.3$ (see, in particular, Dong et al. 2006). Nevertheless, since most microlensed dwarfs (including this one), have bluer colours than this limit, the method can usually be applied, if necessary.

For the 24 microlensed dwarf stars that have microlensing $(V-I)_0$ colours, including the revised colour for MOA-2010-BLG311S, we find that our spectroscopic temperatures are 80 ± 217 K lower than the ones based on the colour-[Fe/H]-$T_{\rm eff}$ relationships (see Fig. 5a). Note that the colours for the previous microlensing events in Bensby et al. (2010c) were estimated under the assumption that the red clump in the bulge has $(V-I)_0 = 1.05$. Hence, those colours have been adjusted (by adding 0.03 mag) and new effective temperatures were determined. For clarity, all 26 events are listed in Table 3. The Casagrande et al. (2010) calibrations can also be used to see what $(V-I)_0$ colours the spectroscopic effective temperatures correspond to. For the new stars these are listed in Table 3, and the comparison between photometric and "spectroscopic" $(V-I)_0$ colours are shown in Fig. 5. On average the spectroscopic colours are in good agreement with the ones from microlensing techniques being only slightly lower (the difference is 0.02 ± 0.07 mag, see Fig. 5b).

This difference is due to that we now use the calibrations by Casagrande et al. (2010), while we in Bensby et al. (2010c) used the ones by Ramírez & Meléndez (2005). If we were to use the Ramírez & Meléndez (2005) calibrations the difference would be 0.00 ± 0.06 mag. This means that the $(V-I)_0$ value for the bulge red clump that was revised from 1.05 to 1.08 in Bensby et al. (2010c) could be revised back again to 1.06.

4. Results

4.1. The metallicity distribution

In Fig. 6a we show the MDF for our sample of 26 dwarf stars in the bulge. Since the typical error in [Fe/H] is about 0.1 dex, we choose a bin size for the histogram of 0.2 dex. This ensures that any feature that we detect in the distribution is not due to error statistics, i.e., features that could originate from the mea-

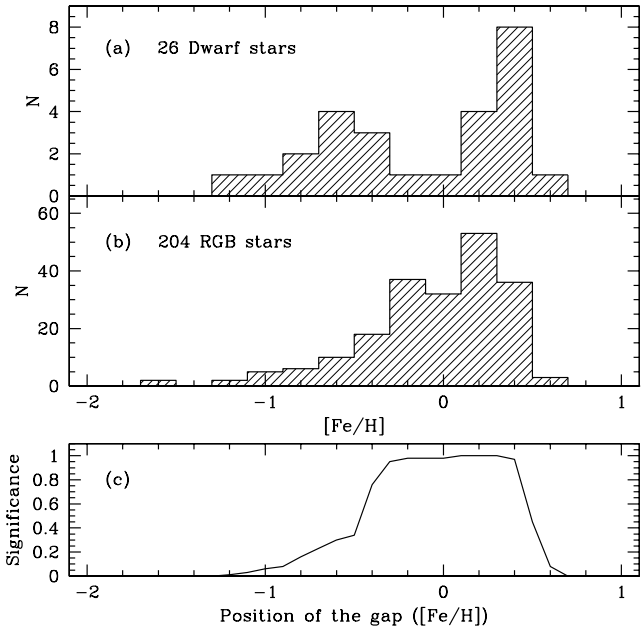

Fig. 6. a) MDF for our 26 microlensed dwarf stars in the bulge. **b)** MDF for 204 RGB stars in the bulge, from Zoccali et al. (2008). **c)** The significance for the failure of reproduce a gap vs. position of a gap in the dwarf star MDF (see explanation in Sect. 4.1).

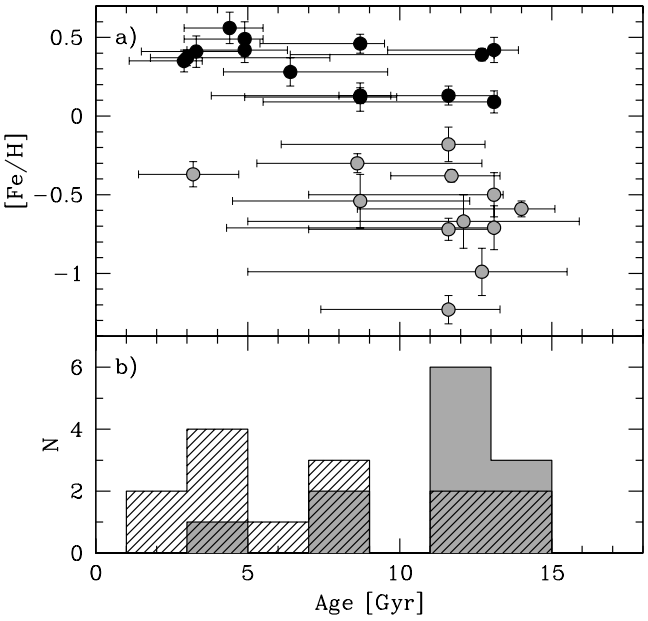

Fig. 7. *Top panel* show ages versus [Fe/H] for the now in total 26 microlensed dwarf and subgiant stars in the Bulge. Stars with [Fe/H] > 0 are marked with black circles and stars with [Fe/H] < 0 with grey circles. *Bottom panel* shows age histograms for the metal-rich stars (hatched histogram) and metal-poor stars (grey histogram).

surement uncertainties are suppressed by the size of each bin. We note that this MDF appears bimodal with peaks at [Fe/H] ≈ -0.6 and $\approx +0.3$ dex, and a gap of only two stars at [Fe/H] ≈ -0.1. In Fig. 6b, for comparison, we show the MDF for 204 RGB stars in the bulge from Zoccali et al. (2008). Given that the MDF for the RGB stars only has one prominent peak (although asymmetric), there is a significant difference between the RGB and the dwarf star MDFs. A Kolmogorov-Smirnov test between the two distributions yields a p-value of 0.11. Even though this is not low enough to reject the null-hypothesis that the MDFs are drawn from the same distribution, under the commonly used limit of 0.05, it is low enough to warrant further investigation.

The most prominent difference is the deficiency of stars in the dwarf star MDF, situated almost where the RGB MDF peaks. The question we ask is: what is the probability of obtaining such a deficiency, similar to the one in the dwarf star MDF, if 26 stars are drawn randomly from the RGB MDF? To answer this question, we construct a simple significance test. First, we draw 26 stars randomly from the RGB MDF. Given that there are 204 stars in the RGB sample, we assume the RGB MDF to be representative of the complete underlying MDF. Next, we check if the sample of 26 randomly drawn stars has a deficiency of stars in the MDF at [Fe/H] = x. We define the deficiency of stars in the MDF as a gap with two stars or less in a metallicity range of 0.3 dex (see Fig. 5a). The gap in Fig. 6 spans about 0.4 dex. However, given that the typical error in [Fe/H] for the dwarf stars is about 0.1 dex, we use a range of 0.3 dex. We iterate this process 10^5 times. We define the significance as the fraction of iterations that fail to reproduce a gap in the randomly generated dwarf star MDF. Finally, we sample over the position of the gap, x, from [Fe/H] = −2 to [Fe/H] = +1 in steps of 0.1 dex.

Figure 5c shows our result from the test. As can be seen, the existence of a gap of stars in the dwarf star MDF at [Fe/H] = −0.1 is unlikely. This indicates that the gap in the MDF is most likely not caused by low number statistics. Additionally, we ran the test with a gap range of 0.2 and 0.4 dex and found that it did not affect the result significantly. Given the possibility of systematic offsets in [Fe/H] for giants and dwarfs, how would a shift in the giant MDF affect the significance level as a function of [Fe/H]? As we sample over all [Fe/H] in the test above, the only effect of shifting the giant MDF is a shift of the significance curve in Fig. 6 by the same amount.

4.2. Ages and metallicities

Figure 7a shows the age-metallicity diagram for the 26 microlensed dwarf and subgiant stars. At sub-solar metallicities the stars are predominantly old with ages between 9 and 13 Gyr (see Fig. 7b), and no apparent trend of increasing or decreasing ages with [Fe/H] is seen. The average age and 1σ dispersion is 11.0 ± 2.9 Gyr. This is similar to what is found for thick disk dwarfs at the same metallicity in the solar neighbourhood (e.g., Fuhrmann 1998; Bensby et al. 2007).

Furthermore, looking again at the metal-poor population, all stars, except MOA-2010-BLG-446S at [Fe/H] = −0.37, seem to have the same age within the errorbars. If we exclude this star the average age becomes 11.7 ± 1.7 Gyr, indicating that the age spread in metal-poor population is indeed very small. Regarding MOA-2010-BLG-446S, we do not rule out the possibility that it is an interloper from the Galactic disk.

The stars at super-solar metallicities on the other hand show a wide range of ages from the youngest disk, being only a few billion years old, to the oldest halo, as old as the Universe (see Fig. 7). The average age and 1σ dispersion is 7.6 ± 3.9 Gyr for the stars at super-solar [Fe/H].

If the ages are weighted by the inverse squares of their errors, the average ages and 1σ dispersions become 5.9 ± 3.4 Gyr for the metal-rich stars, and 11.7 ± 1.5 for the metal-poor stars (9.5 ± 4.2 Gyr when including MOA-2010-BLG-446S).

4.3. Absolute magnitudes

In order to further investigate whether our microlensed dwarf and subgiant stars are indeed in the Bulge, we have compared the absolute I magnitudes obtained from the microlensing photometry with the absolute magnitudes obtained from the spectroscopic stellar parameters.

The spectroscopic absolute magnitudes were obtained with the same methods and the same set of isochrones employed to determine the ages (see Sect. 3). The absolute magnitudes from the microlensing technique, $M_{I,\mu lens}$, were obtained by comparing the instrumental I magnitude of the microlensing source, $I_{instr,s}$, with the instrumental I magnitude of the bulge red clump, $I_{instr,clump}$, assuming that the absolute magnitude of the clump is $M_{I,clump} = -0.15$, i.e.

$$M_{I,\mu lens} = I_{instr,s} - I_{instr,clump} - 0.15 \quad (3)$$

This means that the $M_{I,\mu lens}$ will exactly equal $M_{I,\mu source}$ if:

1. The instrumental clump centroid is correctly measured. [Clump centroids are probably accurate to about 0.1 mag. This is the typical measured difference in the clump centroids of different data sets of the same field and then transformed from one to another.]
2. The instrumental source magnitude is correctly measured. [In most cases this is extremely accurate (of order 0.02 mag or less).]
3. The extinction towards the source is the same as the mean extinction towards the clump. [Most fields have modest differential extinction. There is very little systematic bias. The random error due to differential extinction is probably less than 0.05 mag.]
4. The absolute magnitude of the bulge clump is $M_{I,clump} = -0.15$. [Note: $M_{I,clump} = -0.25$ is the value that usually has been used in bulge microlensing studies. However, recent studies indicate that it probably is incorrect, and should be -0.15 (D. Nataf, private communication).]
5. The source is at the same distance as the clump. [The sources are certainly *not* at the same distance as the clump. They are thought to be in the bulge, and therefore at a range of distances similar to the range of distances of clump stars. However, the sources must be behind the lenses. Thus, if the latter are in the bulge (thought to be about 60% of lensing events) then the former must be preferentially towards the back of the bulge. Hence, on these grounds alone one would expect them to be of order 0.1 mag behind the clump. However, from Fig. 11 it is clear that the spectroscopic sample is drawn preferentially from positive longitudes, which constitute the near side of the Galactic bar, which has a slope of roughly 0.1 mag deg^{-1}. We take this as indicating a strong bias towards brighter sources (which then require less magnification to enter our sample). Of course, *within* any given line of sight, this bias is working on a much narrower baseline, i.e., the intrinsic dispersion in the bulge depth, which is order 0.15 mag. We therefore estimate that the two biases approximately cancel out, and that there is an intrinsic dispersion of source distances of 0.15 mag.]

Figure 8 shows the difference between the absolute I magnitudes from the two methods versus stellar mass (as determined from spectroscopy). The spectroscopic values are on average higher by -0.13 mag (with a dispersion of 0.56 mag). The error bars represent the uncertainties in the spectroscopic values. Even though the individual points appears to be basically consistent at the 1-σ level, there is a tentative trend in the sense that the spectroscopic values are higher for low masses while microlensing values are higher for high masses.

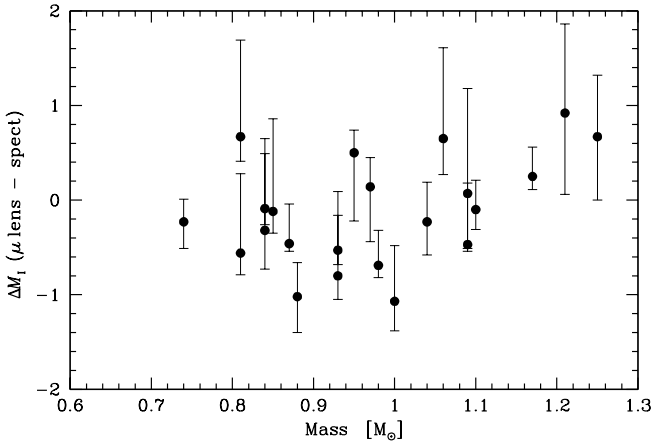

Fig. 8. The difference between the absolute I magnitudes from microlensing techniques and from spectroscopy versus stellar mass (derived from spectroscopy). Error bars represent the uncertainties in the spectroscopic values.

To formally evaluate the significance of the difference between the microlensing and spectroscopic estimates of M_I, we first estimate an error of 0.2 mag in the microlensing M_I values, which is the quadrature sum of the 5 enumerated error sources identified above. We add this in quadrature to the (asymmetric) errors shown in Fig. 8, and evaluate χ^2 as a function of assumed offset. We find $\Delta M_{\rm I} = -0.10 \pm 0.15$, with $\chi^2_{\rm min} = 12.48$ for 21 degrees of freedom. The fact that the mean is within $1\,\sigma$ of zero implies that the sample is consistent with being entirely drawn from bulge stars. Since χ^2 is less than the number of dof, there is no evidence for scatter beyond that due to measurement errors (which includes our estimate of a 0.15 mag dispersion in distances relative to the clump). Of course, this does not prove that all of our sources are in bulge: there could be disk interlopers. However, the fact that microlensing models place the overwhelming majority of lensed sources in the bulge, combined with the demonstrated consistency between the M_I determined from spectra and those determined from microlensing (based on the assumption that they have the same mean distance as the bulge clump) strongly supports a bulge location for the great majority of our sources.

4.4. Colour-magnitude diagram

Figure 9 shows our stars in the HR diagram. We consider the metal-poor and metal-rich stars separately, and we include dereddened colours and absolute magnitudes estimated directly from the spectra (filled circles, see Sect. 3.2) as well as from the micro-lensing technique (open circles, see Sect. 3.3). The two values are connected for each star by a dotted line (note that 4 stars do not have microlensing values, see Table 3). The metal-poor stars (Fig 9a) are spread from the main-sequence to the bottom of the red giant branch. The age of the population of these stars is younger if we consider the magnitudes and colours

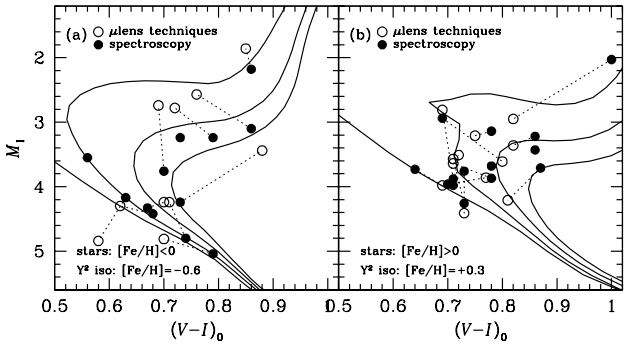

Fig. 9. (a) and (b) show the $(V-I)_0$ versus M_I colour-magnitude diagram using values from microlensing techniques (open circles) and spectroscopy (filled circles). (a) shows the stars with [Fe/H] < 0 and (b) the stars with [Fe/H] > 0. Each CMD also show the Y^2 isochrones (1, 5, 10, and 15 Gyr) from Demarque et al. (2004). For the metal-poor sample the isochrones have [Fe/H] $= -0.6$ and for the metal-rich sample [Fe/H] $= +0.3$. The spectroscopic and microlensing values have been connected with a dashed line for each star (4 stars do not have microlensing values).

derived by micro-lensing techniques (between 5 and 10 Gyr), while, if we use the spectroscopically determined colours and magnitudes, the age is about 5 Gyr larger with a very nicely defined sub-giant branch. Regradless of these differences it is clear that we are dealing with a population that is old.

For the metal-rich stars (Fig 9b) the situation is somewhat different. Here we have no stars that have evolved sufficiently to trace the sub-giant branch. Additionally, the spectroscopy and micro-lensing techniques yield rather similar results for almost all stars. The stars are clustered in the turn-off region and there seems to be both rather young stars (5 Gyr with very little room for a large change) up to stars as old as 10 Gyr. There are quite a few stars that potentially cluster around the 1 Gyr isochrone as well.

In summary, when we consider the high and low metallicity stars as two stellar populations, and study their location in an HR diagram, we see that the metal-poor population is fairly evolved and includes essentially older stars, whilst the metal-rich population is less evolved and tentatively includes some rather young stars.

4.5. Abundance trends

4.5.1. Similarities to the Galactic thick disk

From the analysis of OGLE-2008-BLG-209S, which was the first microlensed subgiant star with a metallicity below solar, we got the first hint from a chemically un-evolved star that the metal-poor parts of the bulge might be similar to those of the Galactic thick disk (Bensby et al. 2009b). In Bensby et al. (2010c) where the sample was expanded to 15 microlensed dwarf and subgiant stars, out of which 7 had [Fe/H] < 0, it was clear that the metal-poor bulge, in terms of both elemental abundance ratios as well as stellar ages, is similar to the Galactic thick disk. With this study we add another five stars with sub-solar metallicities, and another seven with super-solar metallicities. The updated abundance plots are shown in Fig. 10 and it is clear that the new stars further strengthens the similarity between the metal-poor bulge and the Galactic thick disk as seen in the solar neighbourhood. The agreement is almost perfect for all the α-elements and only for the two *s*-process elements Ba and Y are there some discrepancies, and then for only one or two stars at the lowest [Fe/H]. Given the error bars and the fact that it is only 1-2 stars, it is difficult to judge if the differences for Ba and Y are real. We also note the large dispersion in [Zn/Fe] at high metallicities, which most likely is caused by the fact that the Zn abundances for a majority of the stars are based on only one spectral line.

The similarity between the bulge and the local thick disk abundance trends was actually first recognised from studies of K giants (Meléndez et al. 2008) and later by Alves-Brito et al. (2010) and Gonzalez et al. (2011). Recently it has been shown that this similarity also holds when comparing bulge giant stars with K giant stars from the thick disk in the inner parts of the Galaxy (Bensby et al. 2010a).

4.5.2. Rapid enrichment and time scale for SNIa in the bulge

The high level of α-element abundances relative to Fe are signatures of rapid star formation where massive stars, which have short lifetimes, are the main contributors of chemical enrichment of the interstellar medium when they explode as core collapse SNe produce and expel large amounts of α-elements (see, e.g., Ballero et al. 2007b). This will result in high [α/Fe] ratios at low [Fe/H], and we see this for the microlensed dwarf stars at [Fe/H] ≤ -0.4. Once low- and intermediate-mass stars starts to play a significant rôle in the chemical enrichment, through the explosions of SNIa, which produce relatively little of the α-elements, there will be a downturn (knee) in the [α/Fe]–[Fe/H] abundance plot. This is what we see for the microlensed bulge dwarfs at [Fe/H] ≈ -0.4. This means that the star formation in the bulge continued for at least as long as it takes for the SNIa to contribute significantly to the build-up of elements. Estimates of the SNIa time scale depends on the type of environment and ranges from a few hundred million years to 1-2 billion years (e.g., Matteucci & Recchi 2001). In Fig. 7 we see that the bulge dwarfs with sub-solar [Fe/H] predominantly have ages around 10 Gyr, and the lack of an age-metallicity relation for the metal-poor dwarfs (Sect. 4.2) could indicate that SNIa started to contribute to the chemical enrichment soon after star formation started in the bulge. Even though the internal measurement errors in the old stars of the sample is still quite large to be constraining timescales of 100 Myr versus 1 Gyr, this could mean that the timescale for SNIa in the bulge was short. If not, the stars with [Fe/H] just above the knee would have been significantly younger than those on the plateau, but they are not. A short time-scale of a few hundred million years for SNIa is found for elliptical galaxies while the time-scale in the disks of spiral galaxies are a few billion years (e.g., Matteucci & Recchi 2001). Given the similarities we see between the metal-poor bulge and the thick disk it is worthwhile to mention that the thick disk in the solar neighbourhood shows a possible age-metallicity relation (Bensby et al. 2004a; Haywood 2006; Bensby et al. 2007), with the stars that are more metal-rich than the knee having ages that are 1 to 2 Gyr younger than those more metal-poor than the position of the knee. Now, we have only 1-2 microlensed dwarf stars with $-0.4 \lesssim$ [Fe/H] $\lesssim 0$, and it might well be, once we have a larger sample, that those stars turn out to be, on average, younger than the more metal-poor ones. Also note that there is a possibility that the lack of an age-metallicity relation could be due to a lot of mixing (either caused by the bar, or caused by the merging of sub-clumps). Such mechanisms have been proposed to be responsible for both the observed age-velocity relation and

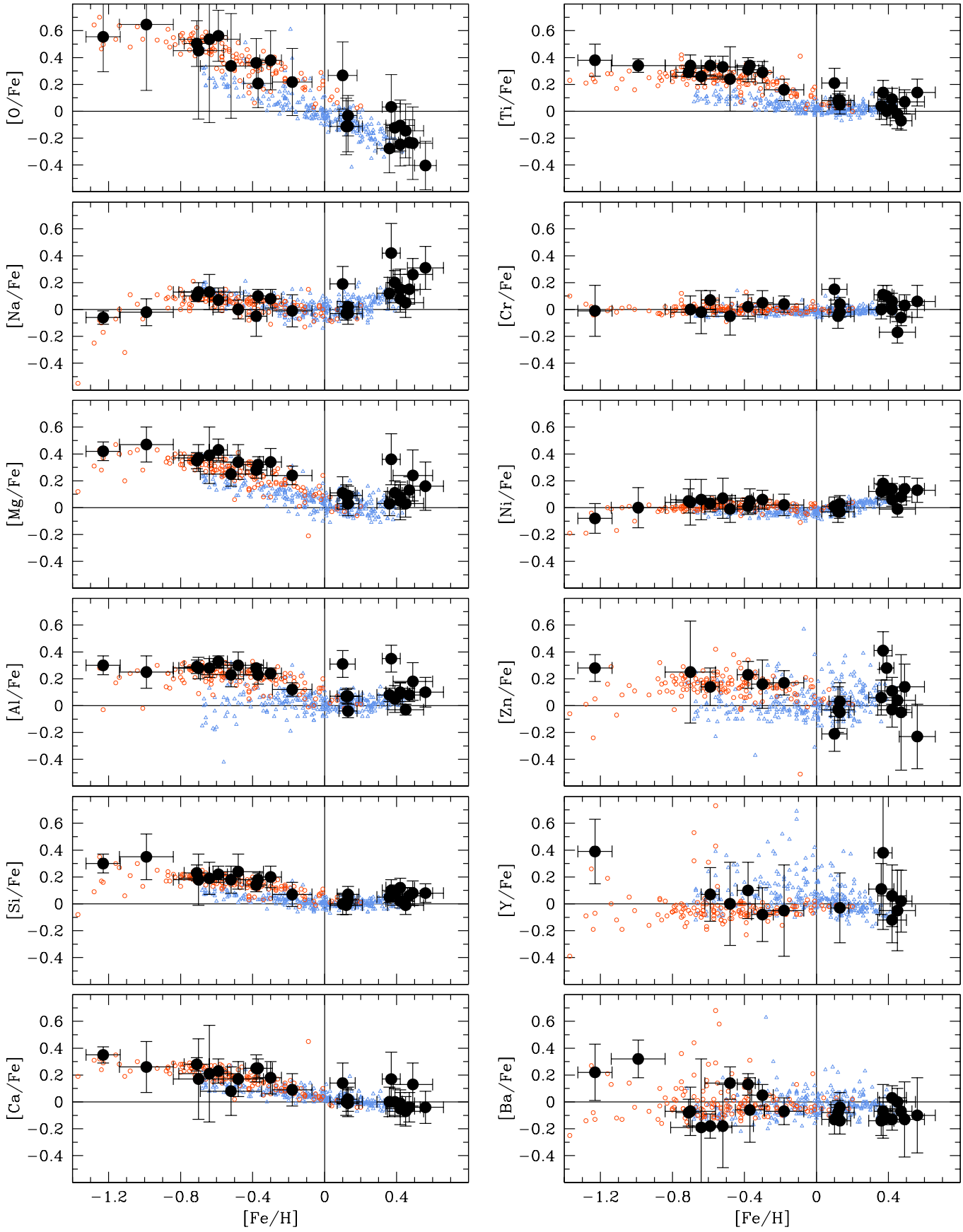

Fig. 10. Filled bigger circles show the abundance results for 25 of the 26 microlensed dwarf and subgiant stars in the Bulge (only stellar parameters were determined for the star from Epstein et al. 2010 that we analysed in Bensby et al. 2010c). Thick disk and thin disk stars from (Bensby et al. 2003, 2005, and in prep.) are shown as small circles red and blue circles, respectively. The error bars represent the total uncertainty in the abundance ratios and have been calculated according to the prescription in Epstein et al. (2010), see Sect. 3.

the absence of age-metallicity relation in the solar neighbourhood (e.g., Minchev & Famaey 2010).

4.5.3. The metal-rich bulge

Regarding the metal-rich bulge, most stars seem to follow the trends as outlined by the thin disk as seen in the solar neighbourhood. However, there are two stars that have elevated abundance ratios that stand out: MOA-2010-BLG-523S at [Fe/H] = +0.09 and MOA-2010-BLG-259S at [Fe/H] = +0.37. From Table 2 we see that these are two of the more evolved stars in the sample. In order to investigate whether the unusually high Na abundances in MOA-2010-BLG-523S and MOA-2009-BLG-259S for their metallicities could be due to the assumption of LTE, we have performed 1D non-LTE calculations following Lind et al. (2011) for the four employed Na I lines. We find that while the non-LTE effects are significant (−0.1 dex) they are essentially the same in all our targets as well as in the Sun, leaving our derived LTE-based [Na/Fe] ratios unaffected. Non-LTE can thus not explain the atypical Na abundances of these two stars. Another possibility could be that the stellar parameters for these stars are erroneous. In order to bring down the [Na/Fe] ratio from +0.19 to zero for MOA-2010-BLG-523S, and to bring down [Na/Fe] ratio from +0.4 to +0.2 for MOA-2009-BLG-259S, we need to increase the effective temperatures with more than 500 K or increase the surface gravities by ∼ 1 dex. As the current temperatures of 5250 K and 4953 K well reproduce the wing profiles of their Hα lines, it is unlikely that erroneous effective temperatures are responsible for the high abundance ratios that we see for some elements in this star. Also, both of these stars have more than 10 Fe II lines measured and the Fe I-Fe II ionisation balances are well constrained, making a shift of 1 dex in surface gravity unlikely. For now we have to accept the fact that these two stars show elevated levels for some elements that does not agree with the other microlensed bulge dwarf stars at similar [Fe/H].

Notable is that the uprising trends of [X/Fe] with [Fe/H] at very high metallicities that are seen for the disk stars for many elements, e.g., [Na/Fe], [Al/Fe], and in particular the iron-peak element [Ni/Fe], is also present in the microlensed bulge dwarfs (see Fig. 10).

We furthermore note that some of the characteristics of MOA-2009-BLG-259S and MOA-2010-BLG-523S (high Na and Al) seem typical of second generation globular cluster stars (e.g., Carretta et al. 2009). Stars resembling globular cluster second generation stars have been found in the halo (Martell & Grebel 2010) and their eventual presence in the bulge might gauge the role that globular clusters had, through losing stars and/or disintegrating in the formation of the bulge. However, Martell & Grebel (2010) have not analysed O, Na, Mg, and Al, so it is still to be proved whether their sample indeed originated from globular clusters. Also, a connection with the globular cluster O-Na anti-correlation for MOA-2009-BLG-259S and MOA-2010-BLG-523S is unlikely given that their O, Na, Al, and Mg abundances are all high (and several other elements too for one of the two stars).

4.6. Positions and radial velocities

Figure 11a shows the positions on the sky for the full sample of microlensed dwarf stars in the bulge. They are all located between galactic latitudes −2° to −5°, similar to Baade's window at (l, b) = (1°, −4°). The reason why most stars are located at positive galactic longitudes and negative latitudes is related

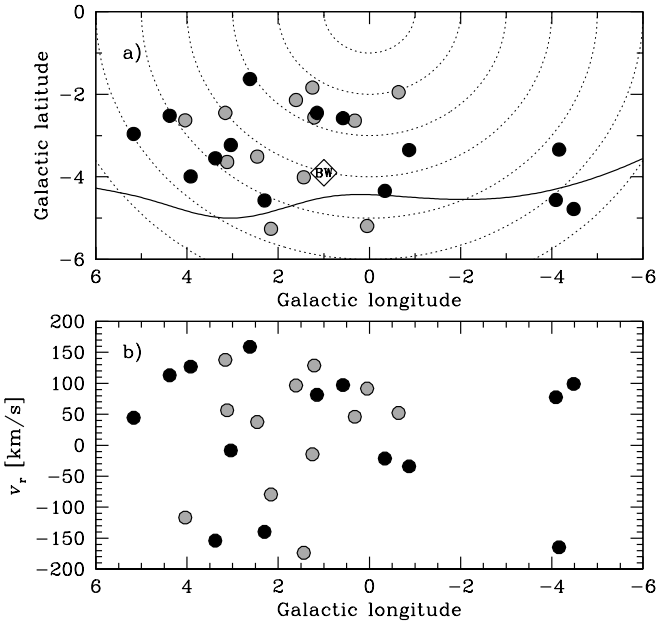

Fig. 11. Positions, radial velocities, and metallicities for the now in total 26 microlensed dwarf and subgiant stars. Grey circles mark stars that have [Fe/H] < 0 and black circles those that have [Fe/H] > 0. The curved line in (a) shows the outline of the southern Bulge based on observations with the COBE satellite (Weiland et al. 1994), and the concentric dotted lines show the angular distance from the Galactic centre in 1° intervals.

to the extinction / geometry of the bulge. As shown in, e.g., Kerins et al. (2009), the optical depth, based on stars, is higher in these regions and therefore the chances for microlensing to occur is higher here. Also, MOA and OGLE have so far mainly surveyed the bulge at negative latitudes as these are regions of lower extinction.

We find that there is essentially no difference in the velocity distributions between the metal-poor and metal-rich samples (see Fig. 11b). The average velocities are almost identical, 21.9 ± 98.7 and 19.7 ± 109.0 km s^{-1} for the two samples. The high velocity dispersion is typical for what has been seen in large surveys of the bulge, for instance the BRAVA survey, which observed and determined radial velocities for several thousand giants (Howard et al. 2008). They found velocity dispersions ranging between 80 − 120 km s^{-1} at these galactic longitudes.

4.7. Lithium abundances in the bulge

As we reported in Bensby et al. (2010b), MOA-2010-BLG-285S is the first metal-poor dwarf star for which Li has been clearly detected in the Galactic bulge. It has a Li abundance which is fully consistent with what is seen in other metal-poor dwarf stars in the Galactic disk and halo at this effective temperature and metallicity (e.g., Meléndez et al. 2010). Figure 12a shows that the star lies on the metal-rich end of the Li Spite plateau (Spite & Spite 1982). Combined with its old age, MOA-2010-BLG-285S is an excellent confirmation that the bulge did not undergo a large amount of Li production or astration in its earliest phases.

The Li abundances in the other five more metal-rich dwarf stars, in which it could be measured, show a wide range,

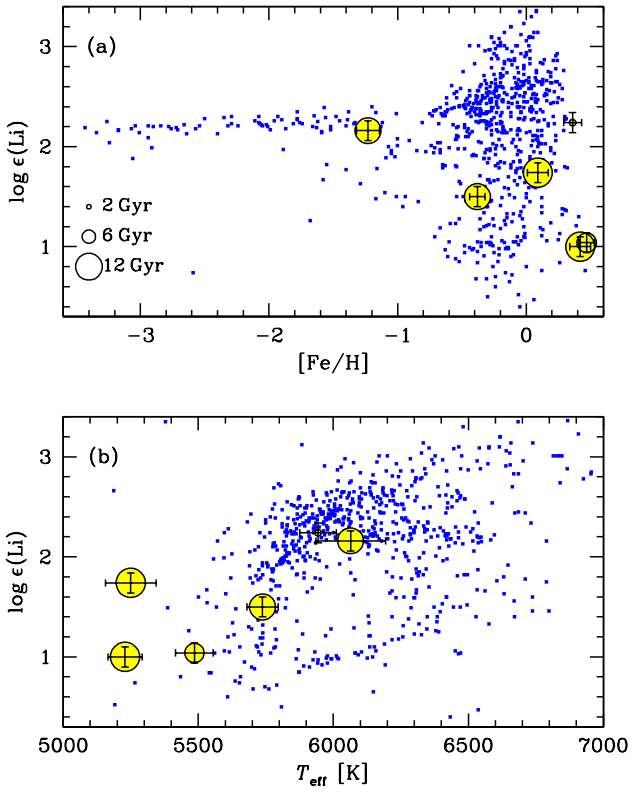

Fig. 12. (a) Li abundance versus [Fe/H], and (b) versus $T_{\rm eff}$. The large circles indicate the microlensed bulge dwarfs listed in Table 6. The ages of the stars have been coded by the sizes of the circles as indicated in (a). Comparison data (small blue dots) come from Meléndez et al. (2010), Lambert & Reddy (2004), and Ghezzi et al. (2010a,b).

most of them significantly lower than the Li Spite plateau. MOA-2008-BLG-311S, which has a higher temperature ($T_{\rm eff}$ = 5944 K) than the other metal-rich stars, is the one with the highest Li abundance. Most likely, the Li in these metal-rich stars represent abundances that were obtained by depletion during their main-sequence lifetimes from higher initial values. Observations of intermediate-age solar-metallicity stars both in clusters such as M67 (e.g., Jones et al. 1999) and in the field (e.g., Baumann et al. 2010) show that they have a large range of Li values, which can be explained by a range of ages, masses, and initial rotation values.

The only other detections of Li in the Galactic bulge are from observations of RGB and AGB stars (e.g., Gonzalez et al. 2009) in which the atmospheric Li abundance have been altered. Dwarf and subgiant stars with effective temperatures greater than about 5900 K are the only reliable tracers of Li (e.g., Weymann & Sears 1965; Boesgaard & Tripicco 1986).

5. Why are the dwarf and giant MDFs different?

The MDF is a key observable used to constrain chemical evolution models (e.g., Chiappini et al. 1997; Kobayashi et al. 2006). Therefore it is important to discuss in detail the differences in the MDFs of dwarf and giant stars in the bulge. If the gap in the dwarf MDF is real and if the bulge MDF truly is bimodal, why does the giant MDF not show this bimodality? Below we discuss several possibilities in detail.

5.1. The microlensed dwarf stars are not in the bulge?

In Bensby et al. (2010c) we explored in detail whether the microlensed dwarf and subgiant stars are located in the Bulge region, or in the disk on either this side or the far side of the Bulge. We concluded then that the combination of kinematics, colour-magnitude diagrams and microlensing statistics makes it highly likely that the microlensed dwarfs that we are studying are members of a stellar population that belong in the Bulge. In this study we have further investigated the bulge membership of the microlensed bulge dwarfs. In Sect. 4.3 we determined the absolute magnitudes of the microlensed dwarfs and compared them to those that can be determined from microlensing techniques. We find that the two are in agreement at better than our 1σ measurement error of 0.15 mag. This is consistent with the expectation (based on Galactic microlensing models) that the overwhelming majority of microlensed sources towards these lines of sight are in the bulge.

5.2. Baade's window not representative?

Could it be that the region towards Baade's window is not representative for the Bulge, not even other close-by regions, and that this is the reason for the discrepant MDFs from the RGB and microlensed dwarf star samples? Zoccali et al. (2008) find different MDFs in their fields (b = −4°, −6°, and −12°) and claim that there is a vertical metallicity gradient in the bulge. The Zoccali et al. (2008) RGB comparison sample is located in Baade's window, which indeed is a very small region of the Galactic bulge. The 26 microlensed dwarf stars have a wider spread in l and b. However, their average distance from the Galactic centre coincides very well with Baade's window (see Fig. 11). Also Brown et al. (2010) used WFC3 photometry and two-colour plots to derive MDFs for 4 fields in the bulge including some close to the Galactic plane (b = −2.15°, −2.65°, −3.81°, and −4.72°). They found that K-S tests ruled out the possibility that they were drawn from the same distribution. They were working in reddening-free measurements, and while not as good as spectroscopy, obviously, it is a possible confirmation of MDF variations across the bulge. Interesting, some of their MDFs look quite metal-rich (though they had issues concerning their zero-point) and more double-peaked.

5.3. Strong gradients in the bulge?

The RGB comparison sample in Baade's window from Zoccali et al. (2008) is located 4° from the Galactic plane as well as from the Galactic centre, while our microlensed dwarf stars range 2°-5° from the Galactic plane and 2°-6° from the Galactic centre (see Fig. 11). Would it be possible that there are gradients present in the metal-rich bulge population that are not picked up by the RGB sample in Baade's window? Possibilities include:

– There are two co-existing bulge populations - one metal-poor and one metal-rich. However, there is a very steep spatial abundance gradient in what we pick up as the metal-rich dwarf population, and at the distance of Baade's window the [Fe/H] is much lower than close to the plane or close to the Galactic centre. Hence, the metal-rich stars can not be seen in the RGB sample from Baade's window.

– There is a number density gradient in the metal-rich population, meaning that at the distance of Baade's window the number of very metal-rich stars has dropped and is very low. Hence, the metal-rich population is missing in the RGB sample.

Babusiaux et al. (2010) use the Zoccali et al. (2008) data and they find a metal-rich and a metal-poor population. They mention that the metal-rich group seems to drop out as they move away from Baade's window, perhaps supporting the second possibility wherein the number density of metal-rich stars drops quickly. From the same stellar sample Gonzalez et al. (2011) show that these two populations separate also in their [α/Fe] ratios. However, the fields they are considering are located at $b = -4°$, $-6°$, and $-12°$, is a significantly larger range than that covered by the microlensed dwarf stars ($b = -2°$, to $-6°$, see Fig. 11) within which the effect should be less dramatic. We also note the claim by Rich et al. (2007), which is based on IR spectroscopy, that there is no metallicity gradient in the inner bulge ($|b| < 4°$).

5.4. Uncertainties in the analysis?

The analysis of giants is more difficult than that of dwarf stars. This is because blending is severe for giants, caused by their lower effective temperatures, which will result in spectra with stronger lines from neutral elements and a lot of molecular lines. The blending will become even more severe for metal-rich stars, which could be the reason for spuriously high abundance ratios in some studies (see, e.g., Lecureur et al. 2007). Regarding problems in the analysis of solar-metallicity giants, Santos et al. (2009) reported that their standard analysis of giant stars in open clusters results in a much narrower metallicity distribution (with a total spread between different clusters of only about 0.1 dex) than that obtained using dwarf stars, which show that there is a cluster-to-cluster spread in metallicity about 2.5 times higher than that found using giants. The problem seems to be related to blends by atomic and molecular lines, as the use of the line list by Hekker & Meléndez (2007), which has been checked for blends, results in a total metallicity spread derived from open cluster giants similar to that derived from dwarfs (Fig. 1 in Santos et al. 2009). Thus, standard analysis of giant stars may result in a compression of the MDF for metallicities around solar or higher, perhaps erasing the metallicity gap we have found in the MDF of the bulge.

The RGB star spectra of Zoccali et al. (2008) have a resolution of $R \sim 20000$, whilst our microlensed dwarf stars are observed with $R \sim 40000$ to 60 000. That blending might be a problem in metal-rich giants can be seen in Fig. 13a which shows how the line-to-line dispersion of the Fe abundances for the Zoccali et al. (2008) RGB sample in Baade's window vary with [Fe/H], reaching dispersions of 0.5 dex, and in some cases even higher.

To better account for the large dispersions seen in the RGB sample we have in Figure 13c constructed an alternative MDF for the RGB sample. Instead of plotting a standard histogram, each star is represented by a normalised Gaussian, defined by the specific mean value and error in [Fe/H] for each star. It would have been be good if we had error estimates similar to the ones that were calculated in Sect. 3 for the microlensed dwarfs, but the only information we have from Zoccali et al. (2008) is the line-to-line dispersion for each of the 204 stars in Baade's window and that in average 60-70 Fe I lines have been used to determine the stellar parameters and [Fe/H]. However, Bensby et al. (in prep.) have performed an error analysis following Epstein et al. (2010) for 703 F and G stars (dwarfs, subgiants, and a handful of low-luminosity giants.). It is found that the calculated errors in [Fe/H] correlate with the line-to-line dispersion of the Fe I abundances. As the analysis of a majority of the 703 stars have used many more Fe I lines than the 60-70 that Zoccali et al. (2008) have used, we select a subsample of $\sim$ 100 stars from the 703 stars that have 100 or less Fe I lines measured and used in the analysis. We then perform a simple linear regression between the line-to-line dispersion and the error in [Fe/H] for those stars. This regression line has a constant of 0.044 and a slope of 0.50, allowing us to transform the line-to-line dispersions into estimated errors in [Fe/H] for the 204 RGB stars. This plot is shown in Fig. 13b. It should be cautioned that the spectra used by Zoccali et al. (2008) have lower resolutions and lower S/N than the spectra used by Bensby et al. (in prep.), and that the stellar parameter determination methodology is different (gravity is not a spectroscopically tuned parameter in Zoccali et al. 2008). Additionaly, and most important, the Zoccali et al. (2008) sample consists of giants while the Bensby et al. (in prep.) have analysed dwarf and subgiant stars. However, it is likely that the stellar parameters are less well determined when the line-to-line scatter is higher.

The total MDF curve shown in Fig. 13c is then the sum of the Gaussians for all 204 RGB stars, normalised to unit area. It is interesting to see how the large uncertainties smears the MDF, and especially, now showing a less steep drop-off at the metal-rich end. The question now is what happens if the same type of uncertainties are added to the sample of microlensed dwarf stars? Can it amount for an erasure of the gap such that the dwarf MDF resembles the RGB MDF?

Assigning each star in the microlensed dwarf sample an uncertainty given by the dashed line in Fig. 13b, we then construct a normalised gaussian for each of the 26 microlensed dwarf stars. These are merged to form a new MDF for the microlensed dwarf sample, and is shown in Fig. 13d. Although the double-peak still is present, it is clear that it has been smeared out. However, the double-peak remains. Hence, we can not blame uncertainties in the giant analysis to be the sole source for the discrepant MDFs, unless the error consists in a compression of the [Fe/H] values (see discussion earlier).

5.5. Disk contamination in RGB sample?

A certain degree of contamination in the RGB sample in Baade's window is expected. Based on the Besançon model of the Galaxy (Robin et al. 2003), Zoccali et al. (2008) estimated a contamination of 10 – 15 % in their RGB sample in Baade's window, divided more or less equally between foreground thin disk stars, located 2 – 5 kpc from the Sun, and thick disk stars located within the bulge. The estimation of the thick disk contamination is based on the assumption in the Besançon model that the thick disk follows an exponential radial distribution that peaks in the Galactic centre. As also stated in Zoccali et al. (2008), these contaminations are poorly determined as we know very little about the stellar populations in the inner Galactic disk, and essentially nothing about possible thin and thick disk stellar populations within the bulge. We therefore find it worthwhile to investigate how much contamination is actually needed for the microlensed dwarf MDF and the Baade's window RGB MDF to agree.

The bulge has a radius of about 1.5 kpc (Rattenbury et al. 2007), meaning that the foreground disk stars, if they are located in front of the Bulge, should be located, at most, approximately 6 kpc from the Sun. Baade's window is located at $b = -4°$, which

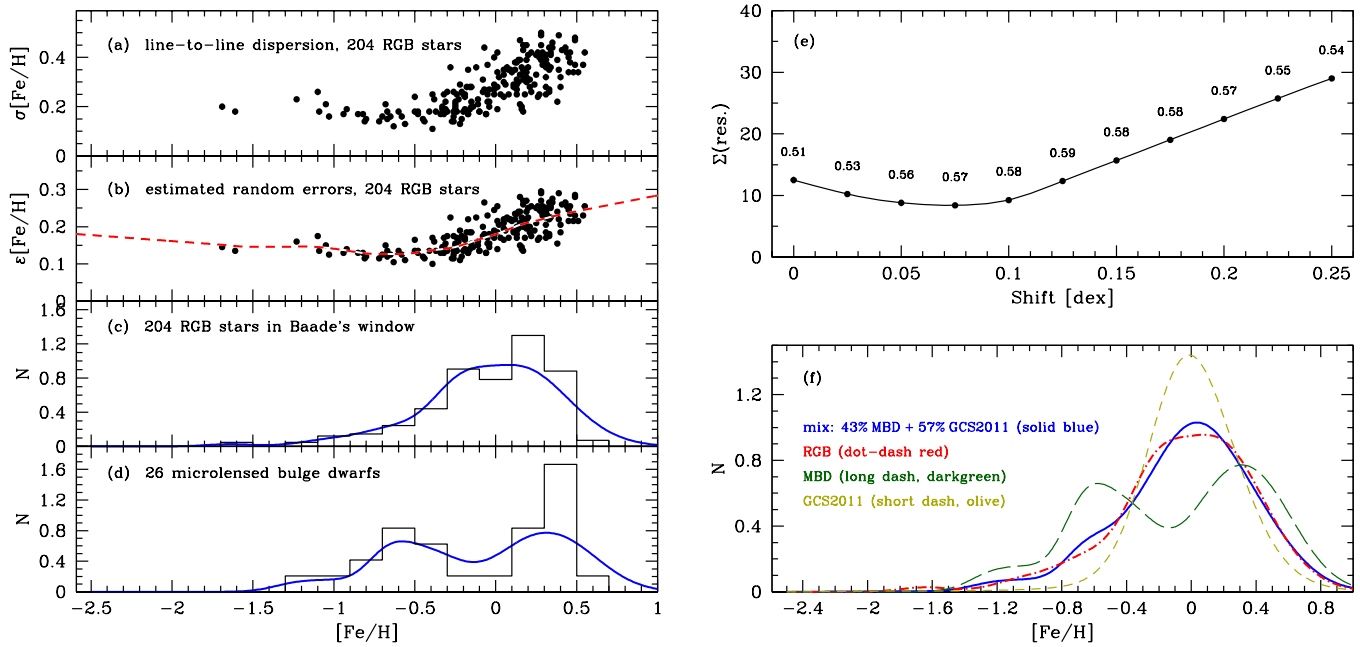

Fig. 13. (a) Line-to-line dispersion of Fe I abundances for the 204 RGB stars from Zoccali et al. (2008); (b) The estimated random errors of the 204 RGB stars from Zoccali et al. (2008). Dashed red line represents the running median (extrapolated outside the data limits); (c) The MDF for the 204 RGB stars. The blue line is a smoothed version where each star is represented by a Gaussian having with a width equal to the estimated random error as shown in (b); (d) The MDF for the microlensed dwarf stars. The blue line is a smoothed version where each star is represented by a Gaussian with a width as given by the dashed line in (b); (e) shows how the sum of the minimum residual between a joint disk GCS and microlensed dwarf MDF and the RGB MDF vary with the shift of the GCS disk sample. For each value, the fraction of the GCS disk MDF is shown. The minimum sum of residuals is reached when the disk GCS MDF is shifted +0.075 dex, and when the fraction of GCS disk MDF is 57 %. The MDFs and the smeared MDFs for the RGB sample in Baade's window (f) The smoothed MDFs for the RGB sample (red dash-dotted line), the microlensed dwarf sample (green long-dashed line), the GCS2011 disk sample (olive coloured short-dashed line). The solid blue line shows the mix of the MDFs from the GCS2011 disk sample and the microlensed dwarf sample that best match the RGB MDF. All MDFs have been normalised to unit area (hence *N* on the ordinates are arbitrary numbers).

at this distance from the Sun translates into a vertical distance of ∼ 400 pc. Assuming that the inner disk contains both a thin and a thick disk (see first results in Bensby et al. 2010a), and that they have similar scale heights as in the solar neighbourhood, this is a distance from the plane where the thin disk is dominating. Hence, it is likely that if the giant sample is contaminated with foreground stars, it should presumably be by thin disk stars.

Assigning each star an uncertainty in [Fe/H] given by the dashed curve in Fig. 13b, we create two normalised MDFs: one for the bulge (green dashed curve in Fig. 13f.) and one for the disk (olive coloured dashed curve in Fig. 13f.). The normalised bulge MDF is based on the 26 microlensed dwarf stars, and the normalised disk MDF on the disk stars from the re-calibration of the Geneva-Copenhagen Survey by (Casagrande et al. 2011, hereafter GCS2011). In the solar neighbourhood the disk MDF peaks slightly below solar (e.g., Casagrande et al. 2011). As the Galactic disk is likely to exhibit a shallow metallicity gradient (e.g., Maciel & Costa 2010; Cescutti et al. 2007, and references therein) the disk closer to the bulge would therefore have a slightly higher average metallicity. We will therefore leave the shift of the GCS2011 MDF as a free parameter.

We then construct a joint MDF from the smeared out dwarf star MDF and the smeared out GCS2011 disk MDF, with varying fractions of the two (from 0 to 1 in steps of 0.1). Then we compare this mixed MDF with the Baade window RGB MDF (as given in Fig. 13a) and determine for which mixture the sum of the residuals is minimised. This procedure is done for several different metallicity shifts of the GCS2011 disk MDF. The results are shown in Fig. 13e which shows how the minimum sum of the residuals changes with the degree of contamination for eleven different shifts of the GCS2011 MDF. The lowest values are achieved for a shift of approximately +0.075 dex of the GCS2011 MDF and a mix of 57 % GCS2011 and 43 % dwarf MDF. As can be seen in Fig. 13f, the mixed bulge-disk MDF and the RGB MDF are similar and agree quite well. Note that the exact shift of the GCS2011 disk MDF seems to be of little importance. All shifts suggest a disk contamination fraction of 50 to 60 %.

Is such a high foreground contamination of the RGB sample realistic? If 50 to 60% of the bulge RGB samples are actually foreground disk stars, this might be visible in the kinematics of the RGB sample. However, the velocity dispersion (σ_{v_r}) is similar in the RGB sample and in the microlensed dwarf sample. Also stars with disk kinematics would introduce a metallicity-dependent bias in the RGB sample, since the foreground contamination only is significant near solar metallicity (between [Fe/H] of −0.3 and +0.1). However, Babusiaux et al. (2010) found no sign of disk kinematics within that metallicity range. Furthermore, the BRAVA survey RGB stars should also presumably be contaminated by foreground disk stars. However, there is good agreement between the v_r distribution of the microlensed dwarfs and that of the BRAVA giants.

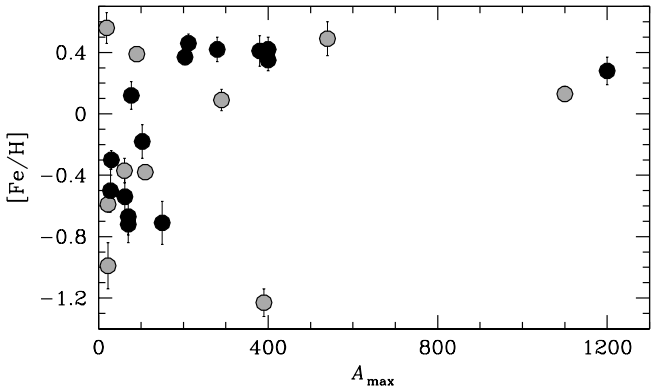

Fig. 14. [Fe/H] versus A_{max}. Grey circles mark the new stars and black circles the stars in Bensby et al. (2010c).

5.6. The magnification puzzle

In Cohen et al. (2010) a peculiar relation between maximum magnification (A_{max}) and [Fe/H] was discovered. Using 16 microlensing events available at that time it was demonstrated that a very strong correlation between metallicity and maximum magnification existed. Several possible explanations were given, but all had to be rejected, leaving the puzzle unsolved. Now, with additional data points in hand, we again look at this issue. As can be seen in Fig. 14 it is evident that most of the events with the highest magnifications have super-solar metallicities, and that lower magnification events dominate at sub-solar metallicities. However, the new data points (grey circles) appears to weaken the relation as we now have high-magnification events at low metallicities and low-magnification events at high metallicities, combinations that were not present in Cohen et al. (2010). A Spearman rank test between [Fe/H] and A_{max} now gives a correlation of 0.42 and a significance that it deviates from zero of 0.033. A Spearman correlation of zero indicates that there is no tendency for [Fe/H] to either increase or decrease when A_{max} increases. This means that we can not rule out the null hypothesis that the two properties are uncorrelated. So, even though there is still a statistical significance that the two parameters are correlated, it is weaker than in Cohen et al. (2010) who found a significance of 0.005, i.e. strongly correlated. More microlensing events are needed in order to resolve whether the A_{max} puzzle is real or not.

In any case, assuming that it is real – how would that affect the microlensed dwarf star MDF? Since all stars observed so far, without exception, has turned out to be either metal-poor *or* metal-rich, the only effect would probably be that the relative sizes of the two peaks change. The most likely scenario is that we are missing more low-magnification events than high-magnification events. If so, that would mean that the metal-poor peak is under-estimated. The gap around solar metallicities would probably persist. To investigate what the effects might be on the results regarding a possible foreground contamination of the RGB sample, we repeat the analysis shown in Fig. 13f with two times as many stars in the metal-poor peak of the microlensed dwarf stars MDF. This results in that the best fit is now found for a mix of 65 % disk stars from GCS2011 (now shifted 0.125 dex) and 35 % microlensed dwarf stars. Thus, if the A_{max} – [Fe/H] puzzle is real, and should be accounted for, the possible foreground contamination of the RGB sample could be even higher.

Table 7. Properties for the metal-rich and metal-poor bulge subsamples[†].

	Metal-poor bulge [Fe/H] < 0	Metal-rich bulge [Fe/H] > 0
N	12	14
[Fe/H]	-0.60 ± 0.30	0.32 ± 0.15
Age	11.7 ± 1.7 Gyr[‡]	7.6 ± 3.9 Gyr
v_r	22 ± 99 km s^{-1}	20 ± 109 km s^{-1}
[α/Fe]	0.29 ± 0.06	0.08 ± 0.05

Notes. [†] The values given in the table are the mean values and their associated dispersions. Also, note that the α-element abundance is here defined as the mean of the Mg, Si, and Ti abundances.
[‡] Excluding MOA-2010-BLG-446S. If this star is included the average age change to 11.2 ± 2.9 Gyr

5.7. Conclusion

In summary, we find no definitive answer to why the bulge MDF look different depending on if it is based on RGB stars or microlensed dwarf stars. Abundance analysis of dwarf stars is certainly coupled to smaller errors and uncertainties than that of giant stars. Also, the resolution and S/N of the microlensed dwarf star spectra are higher than for the RGB stars in Baade's window. Furthermore, statistics show that the microlensed dwarf stars are highly likely to be located in the Bulge region. However, our estimate of the foreground disk contamination is at least four times as high as what the Besançon model used by Zoccali et al. (2008) predicts, and is hard to digest. Given that the knowledge of the inner disk is very poor, and also the fact that the reddening is uncertain and often very patchy, it is clear that it is very difficult to get a handle on the disk contamination in the RGB sample.

6. The origin of the bulge

From our studies of 26 microlensed dwarf and subgiant stars we find that the bulge MDF is bimodal, and Table 7 summarises the properties of the two sub-populations. The metal-poor sample has an average metallicity of [Fe/H] $\approx -0.60 \pm 0.30$, which is in perfect agreement with the mean metallicity that is found for thick disk stars at the solar circle ([Fe/H] = −0.6, Carollo et al. 2010). The metal-rich sample shows a very high-metallicity, and narrow, MDF peaking at [Fe/H] = $+0.32 \pm 0.16$. The metallicity dispersion in the metal-poor sample is twice the dispersion in the metal-rich one. For the metal-poor bulge we find that almost all stars are old with ages in the range 9-13 Gyr, while the stars of the metal-rich population have ages that span from the oldest stars of the Galactic halo (> 12 Gyr) to the youngest stars of the Galactic disk. These age and metallicity differences indicate that the bulge consists of two distinct stellar populations; the metal-poor bulge and the metal-rich bulge, respectively. Furthermore we find that the abundance trends of the metal-poor bulge is similar to those of the Galactic thick disk as seen in the solar neighbourhood, i.e., enriched [α/Fe] ratios signalling a formation on short time-scales. The presence of a "knee" in the [α/Fe] abundance plot, coupled with the lack of an age-metallicity relation, could favour a short time-scale for SN Ia in the bulge. The similarity between the metal-poor bulge and nearby thick disk abundance trends are also seen in studies of giant stars (e.g., Meléndez et al. 2008; Alves-Brito et al. 2010; Ryde et al. 2010) and now this similarity has also been seen between bulge giants and inner Galactic disk giants, 3 to 5 kpc from the Sun

(Bensby et al. 2010a, 2011). The abundance trends of the metal-rich population partly resemble those of the thin disk in the solar neighbourhood. We see no difference in the radial velocity distributions of the two populations, both show the same high velocity dispersions that is expected for a bulge population (Howard et al. 2009).

The observational constraints above points to that the Milky Way has a bulge with a complex composition of stellar populations. The similarities between the metal-poor bulge and the thick disk suggest that they might be tightly connected. Possible scenarios could be that the metal-poor bulge formed from an old Galactic disk (secular evolution, evidence for secular origins of bulges have been seen in many external galaxies, e.g., Genzel et al. 2008), that the metal-poor bulge and the old disk formed simultaneously (but separately), or that the metal-poor bulge and the thick disk are indeed the same population. Simulations have also shown that it is possible for thick disks and bulges to form together by rapid internal evolution in unstable, gas-rich, and clumpy disks (Bournaud et al. 2009), which further could explain the similarities between the Galactic bulge and the thick disk. Furthermore, from a differential analysis of K giants at Galactocentric radii 4, 8, and 12 kpc, Bensby et al. (2011) found that it is likely that the scale-length of the thick disk is shorter than that of the thin disk. This has consequences for the relative fractions of thin and thick disk stars in the Galactic plane, implying that in the bulge region the two disks should be equally present at low galactic latitudes. Interestingly, the 26 microlensed bulge stars divide about equally into being either metal-poor or metal-rich (see Fig. 6). Could this mean that what we are seeing is a bulge solely made up of thin and thick disk stars, and that the metal-rich peak in the microlensed bulge dwarf MDF is a manifestation of the inner thin disk? The thin disk is known to show a strong metallicity gradient (see, e.g., Cescutti et al. 2007), and if interpolated (linearly) to the bulge region it would reach [Fe/H] $> +0.5$. A linear relationship all the way to the bulge is unlikely, but the strong gradient indicates that the average metallicity could end up at, or around, the metallicity that we see for the metal-rich peak of the microlensed dwarf MDF ([Fe/H] $\approx +0.3$). The lack of a radial gradient in the thick disk could be explained through radial migration that has had time to wash out abundance gradients in this old population. For the much younger thin disk, radial migration has not had enough time to act, and a radial metallicity gradient is still present. These findings could support the results from the BRAVA survey which claim that there is no evidence of a classical bulge (Shen et al. 2010), but that the Milky Way is a pure-disk galaxy. The formation of the bulge from a two-component stellar disk has recently been modelled by Bekki & Tsujimoto (2011). We note that also Babusiaux et al. (2010) find evidence for two bulge populations. Their results are based on the metallicities from Zoccali et al. (2008), now complemented with kinematics, and they find that the metallicity gradient along the bulge minor axis observed by Zoccali et al. (2008) can be related to a varying mix a metal-rich population with average metallicity of [Fe/H] $= +0.13$ that has bar-like kinematics and a metal-poor population with average metallicity of [Fe/H] $= -0.3$ that has thick disk-like kinematics. Regarding the metal-rich bulge we find a wide range of stellar ages. As also discussed in Babusiaux et al. (2010), this is consistent with a stellar population with old stars from the inner disk that have been re-distributed by the central bar, and whose young stars have formed in star bursts triggered by the central bar.

7. Implications for the bulge IMF

The MDFs based on the microlensed bulge dwarfs and on red giants in Baades window are clearly different. This has important consequences for chemical evolution models, as the MDF strictly constrains which kind of models are plausible. In particular, the peak of the MDF depends on the slope of the initial mass function (IMF). The chemical evolution model of the bulge by Ballero et al. (2007b) is based on the photometric MDF of giant stars by Zoccali et al. (2003) and on the spectroscopic MDF of giant stars by Fulbright et al. (2006). Ballero et al. (2007b) suggested for the bulge an IMF much flatter than in the solar neighbourhood, i.e., an IMF skewed towards high mass stars, to explain the MDF of bulge giants by Zoccali et al. (2003) and Fulbright et al. (2006).

A more recent model by Cescutti & Matteucci (2011), using now the spectroscopic MDF of giant stars by Zoccali et al. (2008), also favours a flat IMF to reproduce the peak of the MDF of bulge giants. However, those conclusions may have to be revised in view of our new MDF based on microlensed dwarf stars. Our MDF has two well-defined peaks, one that we associate with a metal-poor old bulge, and another one at super-solar metallicities associated with a younger population. Hence, the IMF no longer has to be flat to explain a single peaked solar metallicity MDF that was made in 0.5 Gyr, as in the Cescutti & Matteucci (2011) models. To reproduce the bimodal nature of the bulge MDF, probably a normal IMF can be used for the metal-poor bulge, while contributions from Type Ia SN can probably explain the younger metal-rich peak.

Notice that our MDF is still poorly sampled (only about two dwarfs per metallicity bin), thus, in order to provide even firmer constraints on chemical evolution models, it is important to at least double the sample of microlensed bulge stars observed at high resolution and high S/N. This will provide tight constraints on our galactic bulge, and on a broader context will also have important consequences on the modelling of external galaxies (e.g., Ballero et al. 2007a)

8. Summary

With the twelve events presented in this study the sample size of microlensed dwarf and subgiant stars in the Galactic bulge has grown to 26. All stars have been observed with high-resolution spectrographs on 8-10 m class telescopes, which has allowed us to determine detailed elemental abundances for many elements. The following results and conclusions can be drawn with the current sample.

1. The MDF based on the microlensed dwarf and subgiant stars is bimodal with one peak at [Fe/H] ≈ -0.6, one peak at [Fe/H] $\approx +0.3$, and with essentially no stars around solar [Fe/H]. This is in stark contrast to the MDF provided by giant stars in Baade's window which peaks at this exact location.
2. A statistical test shows that it is unlikely to have a gap in the MDF based on the microlensed dwarf stars if the microlensed sample and the giant sample from Zoccali et al. (2008) have been drawn from the same underlying population. We find no definitive answer to why the two distributions look different. Possible explanations include: large uncertainties in the analysis of the giant stars (especially the metal-rich ones); a higher level than predicted contamination of foreground disk giant stars in the giant sample (maybe as high as 60 %); low number of microlensed dwarf stars, the difference will go away once more microlensing events have been observed; a mix of all above.

3. The metal-poor bulge is very similar to the Galactic thick disk in terms of mean metallicity, elemental abundance trends, as well as stellar ages. The metal-rich bulge is complicated, resembling the thin disk in terms of abundance ratios, but the thin disk does not show a wide range in ages. These findings could be evidence of the co-existence of two distinct stellar populations within the bulge, each which might have its own formation scenario.
4. Combining the similarities between the metal-poor bulge and the thick disk with additional evidence from Bensby et al. (2011) and Shen et al. (2010), we speculate that the bulge is purely made from the stellar disk, where the metal-rich bulge would be the manifestation of the inner thin disk. The origin of the metal-rich bulge population might also be coupled to the Galactic bar, including old stars from the inner disk scattered by the bar and younger stars whose formation was triggered by the bar.
5. Li abundances were presented for six of the microlensed stars. One star is located on the Spite plateau ([Fe/H] = −1.23 and $\log\epsilon$(Li) = 2.16), indicating that the Spite plateau might be universal. The other five stars are all metal-rich and show evidence of Li depletion due to their lower effective temperatures.
6. The new events presented in this study have weakened the recently discovered, and un-explained, $A_{\rm max}$-[Fe/H] puzzle. We now have stars at high [Fe/H] that have low $A_{\rm max}$ and stars at low [Fe/H] that have low $A_{\rm max}$. More events are needed to reveal the true nature of this puzzling relation.
7. The recent claims by Cescutti & Matteucci (2011) of a very flat IMF in the bulge is not supported by the MDF and abundance trends as probed by our microlensed dwarf stars.
8. Lastly, using the new colour-temperature calibration by Casagrande et al. (2010) and the now in total 26 microlensing events, we find that the colour of the bulge red clump is $(V-I)_0 = 1.06$.

Acknowledgements. T.B. was funded by grant No. 621-2009-3911 from The Swedish Research Council. S.F. was partly funded by the Swedish Royal Academy of Sciences and partly by grant No. 2008-4095 from The Swedish Research Council. Work by A.G. was supported by NSF Grant AST 0757888. A.G.-Y. is supported by the Israeli Science Foundation, an EU Seventh Framework Programme Marie Curie IRG fellowship and the Benoziyo Center for Astrophysics, a research grant from the Peter and Patricia Gruber Awards, and the William Z. and Eda Bess Novick New Scientists Fund at the Weizmann Institute. S.L. research was partially supported by the DFG cluster of excellence 'Origin and Structure of the Universe'. J.M. thanks support from FAPESP (2010/50930-6), USP (Novos Docentes) and CNPq (Bolsa de produtividade). J.G.C. was supported in part by NSF grant AST-0908139. J.C.Y. is supported by an NSF Graduate Research Fellowship. Work by C.H. was supported by the grant from National Research Foundation of Korea (2009-0081561). T.S. is supported by JSPS20740104 and JSPS23340044. The MOA project is funded by JSPS20340052, JSPS22403003, and JSPS23340064. We would like to thank Bengt Gustafsson, Bengt Edvardsson, and Kjell Eriksson for usage of the MARCS model atmosphere program and their suite of stellar abundance programs. Finally, we thank anonymous referee for many and valuable comments.

References

Alves-Brito, A., Meléndez, J., Asplund, M., Ramírez, I., & Yong, D. 2010, A&A, 513, A35
Asplund, M., Gustafsson, B., Kiselman, D., & Eriksson, K. 1997, A&A, 318, 521
Babusiaux, C., Gómez, A., Hill, V., et al. 2010, A&A, 519, A77
Ballero, S. K., Kroupa, P., & Matteucci, F. 2007a, A&A, 467, 117
Ballero, S. K., Matteucci, F., Origlia, L., & Rich, R. M. 2007b, A&A, 467, 123
Ballester, P., Modigliani, A., Boitquin, O., et al. 2000, The Messenger, 101, 31
Baumann, P., Ramírez, I., Meléndez, J., Asplund, M., & Lind, K. 2010, A&A, 519, A87
Bekki, K. & Tsujimoto, T. 2011, arXiv:1106.4363
Bensby, T., Alves-Brito, A., Oey, M. S., Yong, D., & Meléndez, J. 2010a, A&A, 516, L13
Bensby, T., Alves-Brito, A., Oey, M. S., Yong, D., & Meléndez, J. 2011, ApJ, 735, L46
Bensby, T., Asplund, M., Johnson, J. A., et al. 2010b, A&A, 521, L57
Bensby, T., Feltzing, S., Johnson, J. A., et al. 2009a, ApJ, 699, L174
Bensby, T., Feltzing, S., Johnson, J. A., et al. 2010c, A&A, 512, A41
Bensby, T., Feltzing, S., & Lundström, I. 2003, A&A, 410, 527
Bensby, T., Feltzing, S., & Lundström, I. 2004a, A&A, 421, 969
Bensby, T., Feltzing, S., & Lundström, I. 2004b, A&A, 415, 155
Bensby, T., Feltzing, S., Lundström, I., & Ilyin, I. 2005, A&A, 433, 185
Bensby, T., Johnson, J. A., Cohen, J., et al. 2009b, A&A, 499, 737
Bensby, T., Zenn, A. R., Oey, M. S., & Feltzing, S. 2007, ApJ, 663, L13
Bernstein, R., Shectman, S. A., Gunnels, S. M., Mochnacki, S., & Athey, A. E. 2003, in Proceedings of the SPIE, Volume 4841, ed. M. Iye & A. F. M. Moorwood, 1694–1704
Bessell, M. S. & Brett, J. M. 1988, PASP, 100, 1134
Boesgaard, A. M. & Tripicco, M. J. 1986, ApJ, 302, L49
Bond, I. A., Abe, F., Dodd, R. J., et al. 2001, MNRAS, 327, 868
Bournaud, F., Elmegreen, B. G., & Martig, M. 2009, ApJ, 707, L1
Brook, C. B., Kawata, D., Scannapieco, E., Martel, H., & Gibson, B. K. 2007, ApJ, 661, 10
Brown, T. M., Sahu, K., Anderson, J., et al. 2010, ApJ, 725, L19
Carollo, D., Beers, T. C., Chiba, M., et al. 2010, ApJ, 712, 692
Carretta, E., Bragaglia, A., Gratton, R. G., et al. 2009, A&A, 505, 117
Casagrande, L., Ramírez, I., Meléndez, J., Bessell, M., & Asplund, M. 2010, A&A, 512, A54
Casagrande, L., Schönrich, R., Asplund, M., et al. 2011, A&A, 530, A138
Cescutti, G. & Matteucci, F. 2011, A&A, 525, A126
Cescutti, G., Matteucci, F., François, P., & Chiappini, C. 2007, A&A, 462, 943
Chiappini, C., Matteucci, F., & Gratton, R. 1997, ApJ, 477, 765
Cohen, J. G., Gould, A., Thompson, I. B., et al. 2010, ApJ, 711, L48
Cohen, J. G., Huang, W., Udalski, A., Gould, A., & Johnson, J. A. 2008, ApJ, 682, 1029
Cohen, J. G., Thompson, I. B., Sumi, T., et al. 2009, ApJ, 699, 66
Combes, F., Debbasch, F., Friedli, D., & Pfenniger, D. 1990, A&A, 233, 82
Dekker, H., D'Odorico, S., Kaufer, A., Delabre, B., & Kotzlowski, H. 2000, in Proc. SPIE Vol. 4008, p. 534-545, Optical and IR Telescope Instrumentation and Detectors, Masanori Iye; Alan F. Moorwood; Eds., ed. M. Iye & A. F. Moorwood, 534–545
Demarque, P., Woo, J.-H., Kim, Y.-C., & Yi, S. K. 2004, ApJS, 155, 667
Dong, S., DePoy, D. L., Gaudi, B. S., et al. 2006, ApJ, 642, 842
Edvardsson, B., Andersen, J., Gustafsson, B., et al. 1993, A&A, 275, 101
Epstein, C. R., Johnson, J. A., Dong, S., et al. 2010, ApJ, 709, 447
Feltzing, S. & Gilmore, G. 2000, A&A, 355, 949
Ferreras, I., Wyse, R. F. G., & Silk, J. 2003, MNRAS, 345, 1381
Fuhrmann, K. 1998, A&A, 338, 161
Fulbright, J. P., McWilliam, A., & Rich, R. M. 2006, ApJ, 636, 821
Fulbright, J. P., McWilliam, A., & Rich, R. M. 2007, ApJ, 661, 1152
Gadotti, D. A. 2009, MNRAS, 393, 1531
Genzel, R., Burkert, A., Bouché, N., et al. 2008, ApJ, 687, 59
Ghezzi, L., Cunha, K., Smith, V. V., et al. 2010a, ApJ, 720, 1290
Ghezzi, L., Cunha, K., Smith, V. V., & de la Reza, R. 2010b, ApJ, 724, 154
Gonzalez, O. A., Rejkuba, M., Zoccali, M., et al. 2011, A&A, 530, A54
Gonzalez, O. A., Zoccali, M., Monaco, L., et al. 2009, A&A, 508, 289
Gould, A., Dong, S., Bennett, D. P., et al. 2010, ApJ, 710, 1800
Grevesse, N., Asplund, M., & Sauval, A. J. 2007, Space Science Reviews, 130, 105
Gustafsson, B., Bell, R. A., Eriksson, K., & Nordlund, A. 1975, A&A, 42, 407
Gustafsson, B., Edvardsson, B., Eriksson, K., et al. 2008, A&A, 486, 951
Haywood, M. 2006, MNRAS, 371, 1760
Hekker, S. & Meléndez, J. 2007, A&A, 475, 1003
Howard, C. D., Rich, R. M., Clarkson, W., et al. 2009, ApJ, 702, L153
Howard, C. D., Rich, R. M., Reitzel, D. B., et al. 2008, ApJ, 688, 1060
Janczak, J., Fukui, A., Dong, S., et al. 2010, ApJ, 711, 731
Johnson, J. A., Gal-Yam, A., Leonard, D. C., et al. 2007, ApJ, 655, L33
Johnson, J. A., Gaudi, B. S., Sumi, T., Bond, I. A., & Gould, A. 2008, ApJ, 685, 508
Jones, B. F., Fischer, D., & Soderblom, D. R. 1999, AJ, 117, 330
Jørgensen, B. R. & Lindegren, L. 2005, A&A, 436, 127
Kerins, E., Robin, A. C., & Marshall, D. J. 2009, MNRAS, 396, 1202
Kobayashi, C., Umeda, H., Nomoto, K., Tominaga, N., & Ohkubo, T. 2006, ApJ, 653, 1145
Kormendy, J. & Kennicutt, R. C. 2004, ARA&A, 42, 603
Kupka, F., Piskunov, N., Ryabchikova, T. A., Stempels, H. C., & Weiss, W. W. 1999, A&AS, 138, 119
Lambert, D. L. & Reddy, B. E. 2004, MNRAS, 349, 757
Lecureur, A., Hill, V., Zoccali, M., et al. 2007, A&A, 465, 799

Lind, K., Asplund, M., & Barklem, P. S. 2009, A&A, 503, 541
Lind, K., Asplund, M., Barklem, P. S., & Belyaev, A. K. 2011, A&A, 528, A103
Loebman, S. R., Roškar, R., Debattista, V. P., et al. 2011, ApJ, 737, 8
Maciel, W. J. & Costa, R. D. D. 2010, in IAU Symposium, Vol. 265, IAU Symposium, ed. K. Cunha, M. Spite, & B. Barbuy, 317–324
Maihara, T., Oda, N., Sugiyama, T., & Okuda, H. 1978, PASJ, 30, 1
Martell, S. L. & Grebel, E. K. 2010, A&A, 519, A14
Matteucci, F. & Brocato, E. 1990, ApJ, 365, 539
Matteucci, F. & Recchi, S. 2001, ApJ, 558, 351
McWilliam, A. & Rich, R. M. 1994, ApJS, 91, 749
Meléndez, J., Asplund, M., Alves-Brito, A., et al. 2008, A&A, 484, L21
Meléndez, J., Casagrande, L., Ramírez, I., Asplund, M., & Schuster, W. J. 2010, A&A, 515, L3
Minchev, I. & Famaey, B. 2010, ApJ, 722, 112
Nordström, B., Mayor, M., Andersen, J., et al. 2004, A&A, 418, 989
Pinsonneault, M. 1997, ARA&A, 35, 557
Piskunov, N. E., Kupka, F., Ryabchikova, T. A., Weiss, W. W., & Jeffery, C. S. 1995, A&AS, 112, 525
Pont, F. & Eyer, L. 2004, MNRAS, 351, 487
Rahimi, A., Kawata, D., Brook, C. B., & Gibson, B. K. 2010, MNRAS, 401, 1826
Ramírez, I. & Meléndez, J. 2005, ApJ, 626, 465
Rattenbury, N. J., Mao, S., Sumi, T., & Smith, M. C. 2007, MNRAS, 378, 1064
Rich, R. M., Origlia, L., & Valenti, E. 2007, ApJ, 665, L119
Robin, A. C., Reylé, C., Derrière, S., & Picaud, S. 2003, A&A, 409, 523
Ryde, N., Gustafsson, B., Edvardsson, B., et al. 2010, A&A, 509, A20
Sadler, E. M., Rich, R. M., & Terndrup, D. M. 1996, AJ, 112, 171
Santos, N. C., Lovis, C., Pace, G., Melendez, J., & Naef, D. 2009, A&A, 493, 309
Schönrich, R. & Binney, J. 2009, MNRAS, 399, 1145
Sellwood, J. A. & Binney, J. J. 2002, MNRAS, 336, 785
Shen, J., Rich, R. M., Kormendy, J., et al. 2010, ApJ, 720, L72
Spite, F. & Spite, M. 1982, A&A, 115, 357
Tumlinson, J. 2010, ApJ, 708, 1398
Valenti, J. A. & Piskunov, N. 1996, A&AS, 118, 595
Vogt, S. S., Allen, S. L., Bigelow, B. C., et al. 1994, in Society of Photo-Optical Instrumentation Engineers (SPIE) Conference Series, Vol. 2198, Society of Photo-Optical Instrumentation Engineers (SPIE) Conference Series, ed. D. L. Crawford & E. R. Craine, 362
Weiland, J. L., Arendt, R. G., Berriman, G. B., et al. 1994, ApJ, 425, L81
Weymann, R. & Sears, R. L. 1965, ApJ, 142, 174
White, S. D. M. & Rees, M. J. 1978, MNRAS, 183, 341
Wyse, R. F. G. & Gilmore, G. 1992, AJ, 104, 144
Yoo, J., DePoy, D. L., Gal-Yam, A., et al. 2004, ApJ, 603, 139
Zoccali, M., Hill, V., Lecureur, A., et al. 2008, A&A, 486, 177
Zoccali, M., Lecureur, A., Barbuy, B., et al. 2006, A&A, 457, L1
Zoccali, M., Renzini, A., Ortolani, S., et al. 2003, A&A, 399, 931